# Measurement report: Hygroscopicity of Size-Selected Aerosol Particles in the Heavily Polluted Urban Atmosphere of Delhi: Impacts of Chloride Aerosol

Anil Kumar Mandariya[1,2], Ajit Ahlawat[3], Mohd. M. V. Haneef[1], Nisar A. Baig[1], Kanan Patel[4], Joshua S. Apte[5], Lea Hildebrandt Ruiz[4], Alfred Wiedensohler[3]*, and Gazala Habib[1]*

[1]Department of Civil Engineering, Indian Institute of Technology Delhi, New Delhi, India

[2]now at: Univ Paris Est Creteil and University Paris Cité, CNRS, LISA, F – 94010 Créteil, France

[3]Leibniz Institute for Tropospheric Research (TROPOS), Permoserstraße, 15 Leipzig, Germany

[4]Department of Civil, Architectural and Environmental Engineering, The University of Texas at Austin, Austin, Texas, USA

[5]McKetta Department of Chemical Engineering, The University of Texas at Austin, Austin, Texas, USA

*Correspondence to*: Gazala Habib (gazalahabib@civil.iitd.ac.in) and Alfred Wiedensohler (ali@tropos.de)

**Abstract.** Recent research has revealed the crucial role of winter-time, episodic high chloride (H-Cl) emissions in the Delhi region, which significantly impact aerosol hygroscopicity and aerosol-bound liquid water, thus contributing to the initiation of Delhi fog episodes. However, these findings have primarily relied on modeled aerosol hygroscopicity, necessitating validation through direct hygroscopicity measurements. This study presents the measurements of non-refractory bulk aerosol composition of $PM_1$ from an Aerodyne aerosol chemical speciation monitor and for first-time size-resolved hygroscopic growth factors (Nucleation, Aitken, and Accumulated mode particles) along with their associated hygroscopicity parameters at 90% relative humidity using a hygroscopic-tandem differential mobility analyzer at the Delhi Aerosol Supersite. Our observations demonstrate that the hygroscopicity parameter for aerosol particles varies from 0.00 to 0.11 (with an average of 0.03 ± 0.02) for 20 nm particles, 0.05 to 0.22 (0.11 ± 0.03) for 50 nm particles, 0.05 to 0.30 (0.14 ± 0.04) for 100 nm particles, 0.05 to 0.41 (0.18 ± 0.06) for 150 nm particles, and 0.05 to 0.56 (0.22 ± 0.07) for 200 nm particles. Surprisingly, our findings demonstrate that the period with H-Cl emissions displays notably greater hygroscopicity (0.35 ± 0.06) in comparison to spans marked by high biomass burning (0.18 ± 0.04), high hydrocarbon-like organic aerosol (0.17 ± 0.05), and relatively cleaner periods (0.27 ± 0.07). This research presents initial observational proof that ammonium chloride is the main factor behind aerosol hygroscopic growth and aerosol-bound liquid water content in Delhi. The finding emphasizes ammonium chloride's role in aerosol-water interaction and related haze/fog development. Moreover, the high chloride levels in aerosols seem to prevent the adverse impact of high organic aerosol concentrations on cloud condensation nuclei activity.

**Supprimé:** ive…Aerosol Particles in theat ...

**Supprimé:** unveiled…the crucialpivotal…role of winter-time, episodic high chloride (H-Cl) emissions in the Delhi region, which significantly impactinfluence…aerosol hygroscopicity and aerosol-bound liquid water, thusereby…contributing to the initiation of Delhi fog episodes in Delhi… However, these findings have primarily relied on modeled aerosol hygroscopicity, necessitating validation through direct hygroscopicity measurements. In t…his study presents , we present …he measurements results of bulk aerosol composition …f non-refractory bulk aerosol composition of $PM_1$ from an Aerodyne aerosol chemical speciation monitor ACSM …nd for first-time size-resolved hygroscopic growth factors (Nucleation, Aitken, and Accumulated mode particles) along with their hygroscopic growth factor and …ssociated hygroscopicity parameters at 90% relative humidity (RH) measured …sing a H-TDMA (…H…groscopic-tT…ndem dD…fferential mM…bility aA…alyzs…r)…at the Delhi Aerosol Supersite (DAS) for the first time… Our observations demonstrate indicate …hat the hygroscopicity parameter for aerosol particles varies ($_{KH-TDMA\_90\%}$) ranges…from 0.00 to 0.11 (with an average of 0.03 ± 0.02) for 20 nm aerosol …articles, 0.05 to 0.22 (0.11 ± 0.03) for 50 nm particles, 0.05 to 0.30 (0.14 ± 0.04) for 100 nm particles, 0.05 to 0.41 (0.18 ± 0.06) for 150 nm particles, and 0.05 to 0.56 (0.22 ± 0.07) for 200 nm particles. SurprisinglyRemarkably… our findings demonstrateresults reveal…that the period withcharacterized by…H-Clhigh chloride (H-Cl)…emissions displays notablyexhibits significantly…greathigh…r hygroscopicity (0.35 ± 0.06) in comparisoned…to spans periods …arked by high biomass burning (H-BB)…(0.18 ± 0.04), high hydrocarbon-like organic aerosol (H-HOA)…(0.17 ± 0.05), and relatively cleaner periods (0.27 ± 0.07). This research presents initial study provides first …bservational proof that evidence of aA…monium cC…loride is the main factor behindas the major contributor to…aerosol hygroscopic growth and bound liquid water content in Delhi. The finding emphasizes, which highlights the role of…aA…monium cC…loride's role in aerosol-water interaction and related haze/fog development. MoreoverAdditionally… the high chloride levelscontent…in aerosols seem to prevent appears to …he adverse impactcounteract the negative effects…of high organic aerosol (OA)…concentrationslevels…on cloud condensation nuclei (CCN) ...

## 1. Introduction

The Intergovernmental Panel on Climate Change (IPCC) (Intergovernmental Panel on Climate Change, 2023) reported that the interaction between aerosols and clouds is not completely comprehended, and there are significant uncertainties in gauging global radiative budgets. In order to overcome and elucidate these uncertainties, the role of aerosol hygroscopicity is crucial. Hygroscopicity is a critical factor in comprehendling how aerosol particles functions as cloud condensation nuclei (CCN) and create fog droplets/haze under sub-saturated/nearly saturation conditions, as well as forming cloud droplets at atmospheric supersaturation levels (McFiggans et al., 2006; Topping and McFiggans, 2012). Its comprehension is vital to better predicting the aerosol size distribution and scattering properties with more accuracy in global models under varying atmospheric humidity (RH) conditions (Randall et al., 2007). Hygroscopicity at higher RH results in an increase in the cross-sectional area of the aerosol, leading to efficient light scattering by the aerosol particles (Tang and Munkelwitz, 1994). This phenomenon is primarily dependent on the chemical composition and particle size. Generally, ammonium salts of sulfate, nitrate, and chloride, which are inorganic salts, exhibit high hygroscopicity (Hu et al., 2011; Petters and Kreidenweis, 2007). In contrast, organic aerosols (OAs) have relatively lower hygroscopicity (Jimenez et al., 2009; Kroll et al., 2011), and dust particles and black/elemental carbon particles are known to be hydrophobic (Seinfeld and Pandis, 2006). The increased atmospheric humidity during winter and monsoon seasons promotes the development of more oxidized secondary organic aerosol (SOA) through aqueous-phase (Ervens et al., 2011) and heterogeneous reactions (McNeill, 2015). This process leads to a heightened organic aerosol hygroscopicity (Jimenez et al., 2009; Mei et al., 2013), which negatively impacts the local visibility (Li et al., 2016; Liu et al., 2012). Conversely, aerosol loading has an inverse effect on aerosol hygroscopicity (Mandariya et al., 2020a). In addition, aerosol loading plays a critical role in determining cloud lifetime, which impacts the amount of rainfall in the region (Albrecht, 1989; Lohmann and Feichter, 2005).

Over the past few decades, researchers have extensively measured aerosol hygroscopicity using a hygroscopic tandem differential mobility analyzer (H-TDMA) (Massling et al., 2005; Gysel et al., 2007; Mandariya et al., 2020; Swietlicki et al., 2008; Yeung et al., 2014; Kecorius et al., 2019) and a CCN counter (Bhattu and Tripathi, 2015; Gunthe et al., 2011; Massoli et al., 2010; Ogawa et al., 2016) under sub- and supersaturated conditions, respectively. Petters and Kreidenweis (2007) introduced the hygroscopicity parameter, kappa (κ), to correlate aerosol hygroscopicity with its chemical composition. Hygroscopicity of OA may differ according to their chemical properties such as solubility, extent of dissociation in aerosol water, and surface activity, which can pose

**Supprimé:** -…clouds interaction …s still …ot completely fully …omprehended, and there areunderstood and has…significant uncertainties in gaugingquantifying…global radiative budgets. In order to overcome and elucidate these uncertainties, the role of aerosol hygroscopicity is crucial.Aerosol hygroscopicity plays a pivotal role in overcoming and explaining these Hygroscopicity is a critical factor in comprehendlingcrucial to understand…how the …erosol particles functionsact…as cloud condensation nuclei (CCN) and create forms …og droplets/haze underat …sub-saturated/nearly saturation conditions, as well as forming and …loud droplets at atmospheric supersaturation levels (McFiggans et al., 2006; Topping and McFiggans, 2012). Its comprehensionunderstanding…is vitalcrucial…to better predicting the aerosol size distribution and scattering properties better…ith more accuracy in global models under varying atmospheric humidity (RH) conditions (Randall et al., 2007). Hygroscopicity at higher RH results in atmospheric conditions leads to …n increaseenhanced…in the aerosol …ross-sectional area of the aerosol, leading toresulting in…efficient light scattering by the aerosol particles (Tang and Munkelwitz, 1994). This phenomenon is primarily dependent on theIt mainly depends on particle size and…chemical composition and particle size. Generally, the inorganic salts such as …mmonium salts of sulfate, nitrate, chloride, which are inorganic salts, exhibit highly…hygroscopicity (Hu et al., 2011; Petters and Kreidenweis, 2007).,…In contrast, organic aerosols (OAs) have relatively lower are comparatively less …ygroscopicity (Jimenez et al., 2009; Kroll et al., 2011), andwhile…dust particles and black/elemental carbon particles are known to bestated as…hydrophobic (Seinfeld and Pandis, 2006). Further, t…he increasedelevated…atmospheric RH…umidity during winter and monsoon seasons promotesfavour…the developmentformation…of more oxidized secondary organic aerosol (SOA) throughvia…aqueous-phase (Ervens et al., 2011) and heterogeneous reactions (McNeill, 2015).,…This process leads to a heightened enhancement in …rganic aerosol hygroscopicity (Jimenez et al., 2009; Mei et al., 2013), which negatively impactsadversely impact on…the local visibility (Li et al., 2016; Liu et al., 2012). ConverselyHowever… aerosol loading has an inversely…ea…fects…on aerosol hygroscopicity (Mandariya et al., 2020a). In additionApart from it… aerosol loading plays is also … critical rolefactor…in determining ciding the cloud lifetime of cloud… which impactsaffects the region's…the amount of rainfall in the region quantitatively …

**Supprimé:** has been intensively measured

**Code de champ modifié**

**Supprimé:** counter …nder sub- and supersaturated conditionsion levels… respectively. Petters and Kreidenweis (2007) introduced thea…hygroscopicity parameter, kappa (κ), to correlateassociate…aerosol hygroscopicity with its chemical composition. Furthermore, h…ygroscopicity of associated with …A may differ according to theirpotentially varies with OA …chemical properties such the …

challenges in quantifying OA hygroscopicity (Hallquist et al., 2009; Jimenez et al., 2009). As a result, this introduces further discrepancies in predicted and measured aerosol hygroscopicity. Therefore, there is a requirement to investigate the measurement-based aerosol hygroscopicity of Delhi's atmosphere to gain a better understanding of the recurring occurrences of haze and cloud formations.

In recent decades, rapid economic growth and industrialization in the Indo-Gangetic Plain (IGP) have resulted in significantly poor air quality during the winter season (Wester et al., 2019). Local and regional air pollution issues may potentially affect Delhi during this time (Arub et al., 2020; Bhandari et al., 2020; Gani et al., 2019; Prakash et al., 2018). Recent studies have indicated that chloride significantly contributes to the degradation of air quality in the Delhi region and favors haze/fog formation during winter (Gunthe et al., 2021). Gani et al. (2019) and Rai et al. (2020) support these findings. Trash and biomass burning for heating and waste degradation have been identified as major sources of chloride in Delhi (Rai et al., 2020). A recent study conducted in Delhi revealed that frequent high chloride events promote high levels of aerosol liquid water content under elevated humid conditions. This leads to haze and poor visibility in the city (Chen et al., 2022). Additionally, Gunthe et al. (2021) found that higher chloride levels also enhance aerosol hygroscopicity. However, it is important to note that this particular study was based on theoretical hygroscopicity. Therefore, it is crucial to study the effects of chloride on aerosol hygroscopicity and its ability to increase the amount of aerosol-bound liquid water based on field measurements. In addition, the heavily polluted urban atmosphere, with its highly complex composition, severely limits the hygroscopicity of the aerosol particles. This is particularly evident in cities like Delhi, located in the IGP of India, where air quality deteriorates significantly during haze/fog-dominated periods. To the author's best knowledge, this study is the first to explore the complex atmosphere of IGP in Delhi, India, using aerosol hygroscopicity measured by H-TDMA.

## 2. Experimental Methods

### 2.1 Aerosol Measurements

Real-time measurements of atmospheric aerosols were conducted during winter (February 1, 2020 to March 20, 2020) at Indian Institute of Technology (IIT) Delhi, Block 5. H-TDMA, TROPOS-type Mobility Particle Size Spectrometer (MPSS), and Aerodyne Aerosol Chemical Speciation Monitor (ACSM) from Aerodyne Research, in Billerica, MA were used simultaneously at a height of approximately 15 meters above ground level (a.g.l.) as depicted in Fig. 1. Lab-2 is located 50 meters away from Lab-1. The ACSM is utilized to quantify mass

**Supprimé:** , leads to difficulty in the quantification of OA hygroscopicity,… As a result, this in …ntroducesing…further more …iscrepancies in predicted and measured aerosol hygroscopicity. ThereforeHence… there is a requirementneed…to investigate explore…he measurement-based aerosol hygroscopicity offor…Delhi's atmosphere to gain a better understanding of the frequent…ecurring occurrences of haze and /…loud formations better ...

**Supprimé:** past…decades, rapidfast…economic growth and industrialization in the Indo- …angetic Plain (IGP) have resulted in significantly led to severe…oor air quality during the winter seasontime…(Wester et al., 2019). Delhi is potentially affected by l…ocal and regional air pollution issuesproblems…i…ay potentially affect Delhi during this n winter ...

**Déplacé vers le bas [1]:** (Gani et al., 2019; Rai et al., 2020)

**Supprimé:** have shown …hloride significantly contributesis one of the…predominant factors …o the degradatione…of air quality in the Delhi region and significantly …avorsur the the ...

**Mis en forme :** Anglais (Royaume-Uni)

**Mis en forme :** Anglais (Royaume-Uni)

**Déplacé (insertion) [1]**

**Supprimé:** (…ani et al.,…(2019) and;…Rai et al.,…(2020) support these findings. Trash and biomass burning for heating and waste degradation have been identified as major sources ofare among the main contributors to…chloride in Delhi (Rai et al., 2020). A recent study conducted conducted …n Delhi revealedported…that frequent high chloride events promotes…high levels of aerosol liquid water content under elevated humid conditions. This leadss…to haze and poor visibility in the city (Chen et al., 2022). AIn a…ditionally, Gunthe et al. (2021) found thatshowed…higher chloride levels also …facilitates …nhancement…in …erosol hygroscopicity.,…h…owever, it isthis study…important to note that this particular study was based on theoretical hygroscopicity. Therefore, it is crucialessential…to studyinvestigate…the effectsimpacts…of chloride on aerosol hygroscopicity and its abilitypotential…to increase the amount of enhance …erosol-bound liquid water based on field measurements. In additionMoreover… the hygroscopicity of the aerosol particles in the …eavily urban atmosphere, with itswhich confines to…highly complex composition, severely limits the hygroscopicity of the aerosol particles. This is particularly evident in cities extremely limited, …ike Delhi, located in the situated at Indo Gangetic Plain (…GP)…of,…India, where air quality deteriorates significantlyseverely degrades…during haze/fog-dominated periods. To the author's best knowledge, thise…current …tudy is the first in Delhi, India,…o exploreing…a…he complex atmosphere of IGP in Delhi, India, using aerosol hygroscopicity measured by H-TDMA-measured aerosol hygroscopicity… Hence, it is essential to measure size-resolved aerosol hygroscopicity in Delhi's ...

**Supprimé:** atmospheric aerosol …easurements of atmospheric aerosols were conducted during winter (February 1, 2020 to March 20, 2020) at Indian Institute of Technology (IIT) Delhi, Block 5. simultaneously using Hygroscopic-Tandem Differential Mobility Analyzer (…-TDMA)… TROPOS-type Mobility Particle Size Spectrometer (MPSS ...

concentrations of organic aerosol (OA), ammonium ($NH_4$), sulfate ($SO_4$), nitrate ($NO_3$), and chloride (Cl) in non-refractory particulate matter less than 1 µm (NR-$PM_1$).

The hygroscopic growth of size-resolved particles at 90 % RH was investigated using the HTDMA system in this study. The HTDMA system has been utilized in numerous field campaigns before (Massling et al., 2007; Wu et al., 2013b; Zhang et al., 2016). The HTDMA system (TROPOS, Germany) consists of two Differential Mobility Analyzers (DMAs) of the Hauke-median type (TROPOS, Germany), along with a Condensation Particle Counter (CPC), Model 3772 by TSI Inc. (USA), and a humidifier system situated between the two DMAs. The initial DMA's function is to choose quasi-monodisperse particles at a dry diameter ($D_p$, dry) of 30% RH. Technical abbreviations will be explicated at their first usage. After passing through a humidity conditioner, the humidity of the size-selected particles can be adjusted from 30% to 90% RH by mixing dry air with RH<5% and moist air with ~95% RH via regulating aerosol and sheath air flow (Maßling et al., 2003). The associated uncertainties with RH measurement at 90% RH are 1.0%. The particle hygroscopic growth distribution at a specific humidity and dry size ($D_p$, dry) can be conveniently determined through CPC. There are two humidity sensors (Vaisala) in the system for aerosol flow and sheath flow respectively. The sensors in the second DMA were calibrated automatically every 30 min at 90% RH using 100 nm ammonium sulfate ($(NH_4)_2SO_4$) particles to analyze stability at high RH. The measurement error of the HTDMA depends mainly on RH measurement and control uncertainties within the system (Su et al., 2010). All RH sensors were calibrated using the Vaisala salt kit containing LiCl, NaCl, KCl and so forth, before the measurement campaign. Size calibration for both DMAs involved the application of Latex particles of standard size, 200 nm prior to measurement. The number concentration peak occurred at 203 nm, which attests to the accuracy of DMAs' size selection at 1.5%. The HTDMA system was used to measure the hygroscopic growth factors (HGFs) of particles with $D_p$, dry of five different sizes (20, 50, 100, 150 and 200 nm), at 90% RH. The full scan covering all five sizes had a time resolution of approximately 30 minutes.

Particle number size distributions (PNSDs) and particle volume-size distributions (PVSDs) were measured using a MPSS

**Mis en forme :** Indice

**Supprimé:** In this study, the HTDMA system was used to investigate …t…e hygroscopic growth of size-resolved particles at 90 % RH was investigated using the HTDMA system in this study. . The …he HTDMA system has been previously …tilizs…d in many…umerous field campaigns before (Massling et al., 2007; Wu et al., 2013b; Zhang et al., 2016). The HTDMA system (TROPOS, Germany) is consistsmprised…of two Differential Mobility Analyzers (DMAs),…of the type…Hauke-median type,…(TROPOS, Germany), along with a Condensation Particle Counter (CPC),…Model 3772 by,…TSI Inc.,…(USA)…, and along with … humidifier system lo…ituc…ted between the two DMAs. The role of first…nitial DMA's function is to chooseselect the…quasi-monodisperse particles at a dry diameter ($D_p$, dry) ofwith…30% RH. Technical abbreviations will be explicated at their first usage. After that, the size-selected particles …assing through a humidity conditioner, humidity of the size-selected particles which …an be adjusted from 30% to 90% RH by regulating the aerosol and sheath air flow by …ixing dry air with RH<5% and humid…oist air with ~95% RH via regulating aerosol and sheath air flow (Maßling et al., 2003). The associated uncertainties associated with RH measurement at 90% RH areis…1.0%. The particle hygroscopic growth distribution at a specific humidity and dry size ($D_p$, dry) can be conveniently at a certain humidity can be easily …etermined throughwith…CPC. There are two humidity sensors (Vaisala) in the system for aerosol flow and sheath flow respectively. The humidity …ensors positioned in the second DMA were calibrated automatically every 30 min at 90% RH usingwith…100 nm ammonium sulfate ($(NH_4)_2SO_4$) particles every 30 min at 90% RH …o analyze the…stability at high RH. The measurement error of the HTDMA mainly …epends mainly on RH measurement and control the …ncertaintiesy…in measuring and controlling the RH …ithin the system (Su et al., 2010). Therefore, a…ll RH sensors were calibrated using the Vaisala salt kit compris…ontaining LiCl, NaCl, KCl and so forth,etc.…beforeprior…the measurement campaign. Size calibration for B…oth the …MAss…involved the application of were size calibrated by applying the …atex particles with the…f standard size, of …00 nm prior tobefore the start of the…measurement. The number concentration peak occurred at 203 nm, which attests to the referring to …ccuracy of DMAs' size selection at 1.5%. The HTDMA system was used operated at 90% RH …o measure the hygroscopic growth factors (HGFs) offor…particles with $D_p$, dry of five different sizes (i.e. …0, 50, 100, 150 and 200 nm), at 90% RH. The …

**Supprimé:** Mobility Particle Size Spectrometer (…PSS (TROPOS type)) …

**Supprimé:** A Detailed description of ACSM setup can be found in Arub et al. (2020). ACSM was operated at nearly 0.1 lpm at 1 min time resolution in a temperature-controlled laboratory. ACSM was set to run to measure mass-to-charge ratio (m/z) m/z 10 to m/z 140. The ACSM measures non-refractory particulate matter less than 1µm (NR-$PM_1$). The concentrate $PM_1$ aerosol beam was impacted on the vaporizer at 600 °C and flash-vaporized compounds were subsequently ionized through impact ionization at 70 eV electron and detected with a quadrupole mass spectrometer (Ng et al., 2011). The 200 ms $amu^{-1}$ scan speed and pause setting at 125 for a sampling time (64 s) were set to acquire aerosol mass spectra in ACSM. Detailed operational procedures for the ACSM are explained elsewhere in Gani et al. (2019).

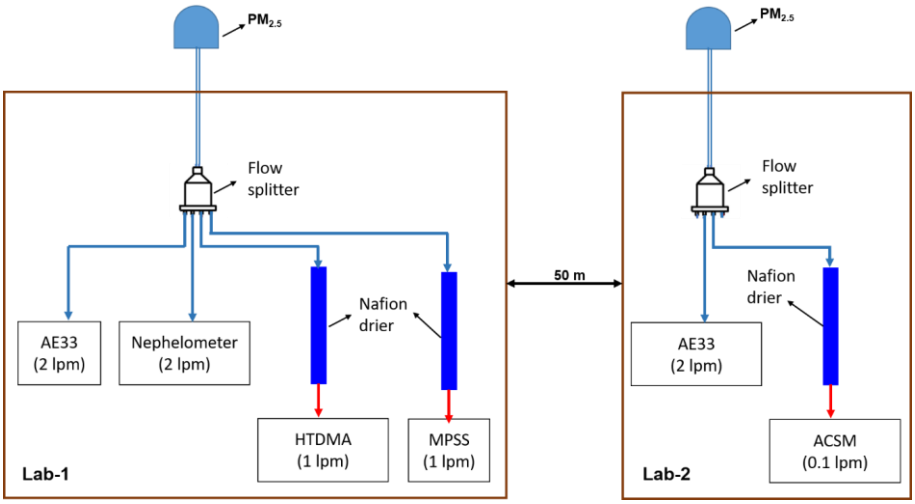


**Figure 1: Schematic diagram of the inlet systems for aerosol sampling instruments. The blue and red sampling lines indicate the ambient air and dehumidified (RH<25%) ambient air, respectively.**

### 2.2 Meteorological and Gas Data

The gas data was obtained from the R.K. Puram-DPCC monitoring station, a continuous ambient air quality monitoring station managed by the central control room for air quality management (Delhi-NCR). The data was downloaded from the CPCB website (https://app.cpcbccr.com/ccr/#/caaqm-dashboard/caaqm-landing/data). R.K. Puram is situated 3.5 km northwest of IIT Delhi. The automatic weather station (Watch Dog 2000 series) continuously measured wind speed (WS), wind direction (WD), temperature (T), and relative humidity (RH). The station is installed on the rooftop of the 9$^{th}$-floor building at IITD.

### 2.3 Data Analysis

#### 2.3.1 H-TDMA

Overall, we conducted 1483 cycles of HTDMA scans. After each cycle, we calculated the percentage difference between the measured and theoretical growth factors (Δq) for 100 nm ammonium sulfate particles. Only those cycles with Δq ≤ ± 5% were included for further data analysis, while the remaining cycles were discarded (Kecorius et al., 2019). As a result, we obtained 1102 HTDMA scan cycles that passed this data quality check. Regarding good scan cycles, we conducted 1449, 1431, 1438, 1470, and 1420 successful H-TDMA scans for particles of sizes 20, 50, 100, 150, and 200 nm particles, respectively, for further analysis. Subsequently, we

**Supprimé:** taken
**Supprimé:** location site
**Supprimé:**
**Supprimé:** controlled
**Supprimé:** gas
**Supprimé:** ere
**Supprimé:** located
**Supprimé:** were continuously measured using an automatic weather station (Watch Dog 2000 series).
**Supprimé:** weather
**Supprimé:** mounted over
**Supprimé:** of the
**Supprimé:** recorded
**Supprimé:** -
**Supprimé:** cycles
**Supprimé:** ward
**Supprimé:** %
**Supprimé:** was calculated after each scan cycle
**Supprimé:** T
**Supprimé:** scan
**Supprimé:** came between
**Supprimé:** ,
**Supprimé:** only carried out for further data treatment, and the rest scans
**Supprimé:** Thus,
**Supprimé:** had
**Supprimé:** -
**Supprimé:** following
**Supprimé:** had
**Supprimé:** good
**Supprimé:** t
**Supprimé:** ze
**Supprimé:** Afterward that

applied TDMAinv Toolkit, a piecewise linear TDMAinv algorithm developed by Gysel et al. (2009) and written in IgorPro, to perform post-data processing on the raw HGF data. The measured distribution function is a smoothed and skewed integral transformation of actual probability density functions for growth factors (GF-PDFs). Gysel et al. (2009) provides a detailed account of the raw data processing in the TDMAinv toolkit for the measurement of real HGFs. The TDMAinv toolkit was successfully employed in various studies across the globe (Gysel et al., 2007; Liu et al., 2012; Sjogren et al., 2007; Wang et al., 2018a), including Kanpur, India (Mandariya et al., 2020a). Furthermore, the RH in DMA2 generally reached the designated 90% value and remained stable within ±1%. However, on occasion, it experienced significant drifts. To address this issue, all growth factors measured between 88% and 92% RH were adjusted to the target value of 90% (HGF_90%) (Gysel et al., 2007) with the kappa-model recommended in the TDMAinv toolkit (Gysel et al., 2009). This approach effectively minimized the RH drifts in DMA2. After conducting scans at target RH for aerosol particles of 20, 50, 100, 150, and 200 nm, 979, 957, 972, 969, and 966 of these scans were respectively corrected. The corrected scans were then averaged for a 60-minute time resolution, resulting in 425, 429, 419, 424, and 417 scans.

Furthermore, using the kappa-Köhler theory (Mandariya et al., 2020a; Petters and Kreidenweis, 2007), we calculated the size-resolved hygroscopicity factors (kappa, κ, say $\kappa_{H\text{-}TDMA\_90\%}$) from the corresponding size-resolved target RH corrected HGFs, based on equation (1).

$$\kappa_{H-TDMA\_90\%} = (HGF\_90\%^3 - 1)\left[\frac{1}{RH}\, exp\left(\frac{4\sigma M_w}{RT\rho_w D_o HGF_{90}\%}\right) - 1\right], \quad (1)$$

Where, $\kappa_{H\text{-}TDMA\_90\%}$ represents the hygroscopicity factor at 90% RH, while HGF_90% is the size-resolve HGF at 90% RH. RH stands for atmospheric relative humidity expressed as a fraction, and σ denotes the surface tension of the aerosol liquid droplet-air interface at the droplet surface measured in N/m, assumed to be nearly to pure water. R represents the universal gas constant, expressed in units of J $K^{-1}$ $mol^{-1}$. $M_w$ denotes the molecular mass of water while T signifies the ambient temperature in Kelvin (K). $\rho_w$ signifies the density of water in kg/$m^3$. $D_o$ denotes the dry mobility diameter of the particle in meters (m).

### 2.3.2 MPSS

The electrical mobility distribution is measured by MPSS and then converted to PNSD in the 8 to approximately 800 nm mobility diameter range. This is achieved by utilizing an inversion algorithm to correct for multiple charged aerosol particles (Wiedensohler, 1988; Pfieffer et al., 2014) and diffusional losses (Wiedensohler et al., 2012; 2018).

**Supprimé:** piecewise linear TDMAinv algorithm, namely…TDMAinv Toolkit, a piecewise linear TDMAinv algorithm written in IgorPro and …eveloped by Gysel et al. (2009) and,…written in IgorPro, to performwas used to do…post-data processing treatment …n the raw HGF data. Because t…he measured distribution function is a skewed and smoothed and skewed integral transformation of the…actual growth factor …robability density functions for growth (GF-PDFs). Gysel et al. (2009) provides A… detailed account description …f the raw data processing in the TDMAinv toolkit to…or the measurement of real HGFs. is described in Gysel et al. (2009). …he TDMAinv toolkit was successfully employedused…in various studies acrossund …

**Mis en forme** …

**Supprimé:** and at

**Code de champ modifié**

**Code de champ modifié**

**Supprimé:** Besides… the RH in the …MA2 generally reachedachieved…the designatedset value of…90% value and remained stable within ±1%,… However, onalthough…occasionally… it experienced significantfaced a more considerable…drifts. To address this issue, A…ll factors measured between 88% and 92% RH were adjusted corrected …o thea…target value of 90% (HGF_90%) (Gysel al., 2007) with using …he kappa-model recommended suggested …n the TDMAinv toolkit (Gysel et al., 2009) to minimize this DMA2 RH drifts… This approach effectively minimized the RH drifts in DMA2. After conductingit…scans,…at target RH for aerosol particles of 20, 50, 100, 150, and 200 nm, 979, 957, 972, 969, and 966 of these scans were respectivelyfound…corrected at target RH for 20, 50, 100, 150, and 200 nm aerosol particles, respectively,… The corrected scans were thenwhich further…averaged for a 60- …inute time resolution, and finally, these numbers reached to…resulting in 425, 429, 419, 424, and 417 scans, respectively …

**Supprimé:** were calculated from the respective…size-resolved target RH corrected HGFs, based on equation (1) using equation (1) kappa-Köhler theory (Mandariya et al., 2020a; Petters and Kreidenweis, 2007) …

**Supprimé:** is…the hygroscopicity factor at 90% RH, while HGF_90% is the size-resolve HGF at 90% RH.,…RH stands foris the…atmospheric relative humidity expressed as ain…fraction, and σ denotei… the surface tension of the aerosol liquid droplet-air interface at the droplet surface measured in N/m, and can be …ssumed to be nearly to pure water.,…R representsis…the universal gas constant, expressed in units of J $K^{-1}$ $mol^{-1}$.,…$M_w$ denotesis…the molecular mass of water while,…T signifiesis…the ambient temperature in Kelvin (K).,…$\rho_w$ signifiesis…the density of water in kg/$m^3$.,…and …$_o$ denotesis …

**Supprimé:** MPSS measures …lectrical mobility distribution, which…is measured by MPSS and then converted to PNSD the 8 to approximately ~…00 nm mobility diameter range. This is achieved by utilizingby applying …

### 2.3.3 ACSM

For a detailed account of the ACSM setup, please refer to Arub et al. (2020). The ACSM operated in a temperature-controlled laboratory at almost 0.1 lpm and 1-minute time resolution. It was set to measure mass-to-charge ratio (m/z) from 10 to 140. The $PM_1$ aerosol beam was concentrated and directed towards the vaporizer at 600 °C. The flash-vaporized compounds were then ionized through impact ionization at 70 eV electrons and detected using a quadrupole mass spectrometer (Ng et al., 2011). The study employed a 200 millisecond $amu^{-1}$ scan speed and a pause setting of 125 for a sampling duration of 64 seconds to collect aerosol mass spectra using the ACSM technique. Refer to Gani et al. (2019) for comprehensive guidance on the ACSM operational procedures. For ACSM calibration and data processing, please refer to Patel et al. (2021). Positive matrix factorization (PMF) was conducted on the data , resulting in a four-factor solution: hydrocarbon-like OA (HOA), biomass burning OA (BBO), less-oxidized OA (LO-OOA), and more-oxidized OA (MO-OOA), as shown in Fig. S1. More information regarding PMF analysis can be found in section S.1 and Fig. S2 of the Supplementary information. Three different events were identified based on the temporal variation of mass concentration peaks of BBOA, HOA, and Cl (see Fig. 2): 1) a high-residential or biomass burning period (H-BB); 2) a high-hydrocarbon-like OA period (H-HOA); and 3) a high-chloride period (H-Cl). Additionally, the "Clean Period" was defined as a period where the $PM_1$ loading was less than the 25$^{th}$ percentiles (≤ 38.7 µg $m^{-3}$) for the sampling period. The event's starting and ending times were determined by the initial increase in concentration and subsequent return to the starting values as the concentration decreased.

### 2.3.4 Derived Secondary Inorganic Salts

The ACSM measures OA, $NO_3$, $SO_4$, $NH_4$, and Cl. A simplified ion-pairing scheme from Gysel et al. (2007) was adopted. However, $NH_4Cl$ was not included in their ion-pairing scheme; therefore, we modified it to integrate ammonium chloride into the calculation. Thus, our modified ion-pairing scheme includes $NH_4Cl$ (ACl), $NH_4NO_3$ (AN), $(NH_4)_2SO_4$ (AS), $NH_4HSO_4$ (ABS), and $H_2SO_4$ (SA) as shown below:

**Case-1 $R_{SO_4}(NH_4\ to\ SO_4) \leq 1$**

$$SA = 98.0795 \times \max\left(0, (n_S - n_A)\right)$$

**Supprimé:** An Aerodyne Aerosol Chemical Speciation Monitor (ACSM, Aerodyne Research, Billerica MA) provided mass concentrations of organic aerosol (OA), ammonium ($NH_4$), sulfate ($SO_4$), nitrate ($NO_3$), and chloride (Cl). Details on…or ACSM calibration and data processing, please refer to are in…Patel et al.,…(2021). We conducted Positive matrix factorization (PMF) was conducted on the data , resulting in and found … four-factor solution: (…ydrocarbon-like OA,…("…OA)"…;…biomass burning OA , "…BBO)A";… less-oxidized OA,…"…LO-OOA),";…and more-oxidized OA "…MO-OOA), to best represent the data set…s shown in Fig. S1. More information regardingFurther details about…PMF analysis can be found are …n section S.1 and Fig. S2 of the Supplementary informationI… Three different events were identified Furthermore, …ased on the temporal variation of mass concentration peaks of BBOA, HOA, and Cl (seein the temporal variation (…Fig. 21…, respectively, three different events were characterized… 1) a hH…gh-residential or biomass burning period (H-BB);…2) a H…igh-hydrocarbon-like OA period (H-HOA);…and 3) a H…igh-chloride period (H-Cl) period… AIn a …

**Mis en forme :** Exposant

**Supprimé:** …ercentiles (≤ 38.7 µg $m^{-3}$) forof …the sampling period. The event's starting and ending times of the event was…ere determinedfined…by the initial increasestarting the increment…in the …oncentration and subsequent return to the starting values asreaching the starting value while …

**Supprimé:** mainly …easures OA, $NO_3$, $SO_4$, $NH_4$, and Cl. Therefore, we adopted a… simplified ion-pairing scheme reported by …ADDIN CSL_CITATION { "citationItems" : [ et al. (2007) did not include …$H_4Cl$ was not included in their ion-pairing scheme; therefore, we elaborated this scheme and made some …odifiedcations…it to integrate in this scheme to include a…ammonium chloride (ACl)…into the calculation. ThusHence… our modified ion-pairing scheme includes $NH_4Cl$ (ACl), $NH_4NO_3$ (AN), $(NH_4)_2SO_4$ (AS), $NH_4HSO_4$ (ABS), and $H_2SO_4$ (SA) asre …

$$\mathrm{ABS} = 115.11 \times \mathrm{n_A}$$

$$AS = 0$$

$$\mathrm{AN} = 0$$

$$\mathrm{ACl} = 0$$

**Case-2 $1 < R_{SO_4} < 2$**

$$\mathrm{SA} = 0$$

$$\mathrm{ABS} = 115.11 \times \left((2 \times \mathrm{n_S}) - \mathrm{n_A}\right)$$

$$\mathrm{AS} = 132.1405 \times (\mathrm{n_S} - \mathrm{n_A})$$

$$\mathrm{AN} = 0$$

$$\mathrm{ACl} = 0$$

**Case-3 $R_{SO_4} \geq 2$**

$$\mathrm{SA} = 0$$

$$\mathrm{ABS} = 0$$

$$\mathrm{AS} = 132.1405 \times \mathrm{n_S}$$

$$\mathrm{AN} = \left(\min\left(\left(\mathrm{n_A} - \left(\frac{\mathrm{ABS}}{115.11}\right) - \left(\frac{(2 \times \mathrm{AS})}{132.1405}\right)\right), \mathrm{n_N}\right)\right) \times 80.0434$$

$$\mathrm{ACl} = \left(\min\left(\mathrm{n_C}, \left(\mathrm{n_A} - \left(\frac{\mathrm{ABS}}{115.11}\right) - \left(\frac{2 \times \mathrm{AS}}{132.1405}\right) - \left(\frac{\mathrm{AN}}{80.0434}\right)\right)\right)\right) \times 53.54$$

Here, "n" represents the number of moles, while "A", "N", "S", and "C" represents the species $NH_4$, $NO_3$, $SO_4$, and Cl. Inorganic salts concentrations were also predicted using the $NH_4$, $SO_4$, $NO_3$, and Cl components of the ISORROPIA v2.1 model. Our results shows a strong correlation and nearly unit slope (0.9999) between the

**Supprimé:** denotes

**Supprimé:** ereas

**Supprimé:** denotes

**Supprimé:** species

**Supprimé:** We also predicted these i

**Supprimé:** from

**Supprimé:** using $NH_4$, $SO_4$, $NO_3$, and Cl

**Supprimé:** We found

calculated and modeled inorganic salts, as presented in Fig. S3. This strongly justifies the new ion-pairing scheme utilized in this study.

### 2.3.5 Windrose and Potential Source Contribution Function (PSCF)

The windrose plot was generated using the openair package in R (http://www.r-project.org, http://www.openair-project.org). An offline based Hybrid Single-Particle Lagrangian Integrated Trajectory (HYSPLIT4) model developed by NOAA/Air Resources Laboratory (ARL)) (Draxler and Hess, 1997) was used to estimate the 48-hour back trajectory of air masses that reached DSL at 500 m above ground for the entire study period at hourly intervals.. The meteorological data used for back trajectories was obtained from ARL's Global Data Assimilation System archive, specifically the GDAS 0.5 degree archive (http://ready.arl. noaa.gov/archives.php). We used these estimated back trajectories and the measured mass fraction of chemical species of bulk aerosol as input in conducting Potential Source Contribution Function (PSCF) analysis. This analysis was carried out with the aid of Zefir (version 3.7), a tool written in Igor Pro (WaveMetrics). The Zefir tool is described in detail elsewhere (Petit et al., 2017). Additionally, this tool was used to create the box plots discussed in the following section. To calculate the aerosol liquid water content (ALWC) as a function of inorganic species mass concentration, ambient T, and RH, the ISORROPIA-II model (Fountoukis and Nenes, 2007) was utilized.

## 3. Result and Discussions

### 3.1 Overview of meteorology, trace gases, and aerosol characterization

Fig. 2 depicts the hourly-resolved temporal changes of various meteorological parameters, including RH, T, WD, and WS, PNSD, PVSD, principal components of non-refractory $PM_1$, and OA, with their corresponding fractional mass contributions. In addition, Fig. S5 exhibits the temporal fluctuations of atmospheric gases, specifically nitrogen oxides (NOx), carbon monoxide (CO), and sulfur dioxide ($SO_2$). Delhi's winter climate is mainly affected by a depression caused by Western Disturbances, resulting in cold waves in the region. The ambient RH and T vary within the range of 24.2% to 96.6% and 9.0 °C to 28.5 °C, respectively. The average values of RH and T are 56.0% ± 18.2% and 18.7 °C ± 4.2 °C, respectively. These fluctuations indicate a shift in Delhi's atmosphere transitions from being damp and chilly in February to dry and relatively warm in March. Nighttime conditions are consistently cooler and more humid than daytime conditions throughout the sampling period. Ambient RH exhibits a diurnal pattern, with a peak occurring during the early morning hours (06:00-07:00) and a valley appearing around midday (13:00-15:00). Conversely, ambient temperature follows an opposing trend, increasing at midday, which can be correlated with higher solar radiation during those hours (refer to Fig. 3a & b). The high

**Supprimé:** l…d inorganic salts, as presented in Fig. S31…,…Thiswhich…strongly justifies the new ion-pairing scheme utilizedadopted ...

**Supprimé:** plotted by…openair in R …ackage in R (http://www.r-project.org, http://www.openair-project.org). The 48-hour back trajectory of air masses reaching Delhi super site (DSL) at 500 m above the ground at every hour for the entire study period was estimated by a…n offline based Hybrid Single-Particle Lagrangian Integrated Trajectory (HYSPLIT4) model developed by NOAA/Air Resources Laboratory (ARL)) (Draxler and Hess, 1997) was used to estimate the 48-hour back trajectory of air masses that reached DSL at 500 m above ground for the entire study period at hourly intervals.. The input…meteorological data used for back trajectories wasere…taken…btained from ARL's the …lobal Data Assimilation System (GDAS 0.5 degree) …rchive, specifically the …DAS 0.5 degree archivemaintained by ARL…(http://ready.arl. noaa.gov/archives.php). We usedFurther, utilizing …these estimated back trajectories and the as input combined with the …easured mass fraction of chemical species of bulk aerosol as input in conducting,…Potential Source Contribution Function (PSCF) analysis was carried … This analysis was carried out with the aidhelp…of a tool called Zefir (versionV…3.7), a tool written in Igor Pro (WaveMetrics). TheDetail description regarding…Zefir tool is described in detailcan be found…elsewhere (Petit et al., 2017). AIn a…ditionally, this tool was used to create the box plots discussed in the followingreported in the subsequent…section. were also plotted with the help of this tool. …o calculate T…he aerosol liquid water content (ALWC) as a function of inorganic species mass concentration, ambient temperature (…)… and ambient relative humidity (…H)… was calculated by ...

**Supprimé:** illustrates…the hourly-resolved temporal changes of variousvariability of…meteorological parameters, including relative humidity (…H)… temperature (…)… wind direction (…D)… and wind speed (…S)… as well as the particle number size distribution (…NSD)… particle volume size distribution (…VSD)… principal components refractory $PM_1$, and organic aerosol (…A)…with their corresponding fractional mass contributions. In A…ddditionally… Fig. S5 displays…xhibits the temporal fluctuationsvariability…of atmospheric gases, such as…pecifically nitrogen oxides (NOx), carbon monoxide (CO), and sulfur dioxide ($SO_2$). Delhi's winter climate is mainly affectedprimarily influenced…by a depression causedgenerated…by Western Disturbances, resulting in cold waves in the region. The ambient relative humidity (…H)…and temperature (…)…vary withexhibit variability in the range of 24.2% to 96.6% and 9.0 °C to 28.5 °C, respectively. The , with …verage values of RH and T are 56.0% ± 18.2% and 18.7 °C ± 4.2 °C, respectively. These fluctuations indicate a shift inthat…Delhi's atmosphere transitions from being dampwet…and chillyold…in February to dry and relatively warm in March. Notably, n…ighttime conditions are consistently tend to be …ooler and more humid thancompared to …daytime conditions throughout the sampling period. Ambient RH exhibits a diurnal pattern, with a peak occurring duringin…the early morning hours (06:00-07:00 hours… and a valley appearing around midday (13:00-15:00 hours…. CIn c…nverselytrast… ambient temperature follows an opposing trend, increasingrising during…at midday, which can be correlated with higher solar radiation during those hours (refer tosee…Fig. 3a & b). The higher ...

ambient temperature and peak $O_3$ concentration observed during midday (see Fig. 3(i)) indicate the possibility of daytime photo-oxidation processes according to research carried out by Nelson et al. (2023). Fig. S6 displays the variation of WS and WD, ranging from 0.0 to 5.6 (with an average of 1.0 ± 1.0) m/s and 4.0 to 345.7 (with an average of 197.1 ± 84.4) degrees from the North, respectively. The majority of wind directions were in the WNW-WSW and E-ESE direction. These patterns indicate that the air quality in Delhi remained relatively stagnant throughout the study period. The measured aerosols are likely to be a result of local emissions and aerosol chemistry.

Throughout the sampling period, ambient trace gases NOx and CO demonstrate notable variability, peaking from local burning activities. During intense biomass burning activities, ambient NOx levels reach a maximum of 421.2 ppb (58.4 ± 61.9). CO concentrations also reach maximum levels during similar periods as NOx, varying from 0.0 to 7.66 ppm (0.58 ± 0.79), as illustrated in Fig. S5. The time-specific changes in the levels of these trace gases are illustrated in Fig. 3 (f, g, h, and i). The graph indicates two crests (06:00-08:00 and 17:00-20:00 hours), which are attributed to local biomass/trash burning emissions that happen in the morning and heavy traffic during nighttime rush hours. Conversely, $SO_2$ demonstrates a distinct pattern, with varying concentrations ranging from 0.46 to 9.55 ppb (4.41 ± 1.20). Notably, it exhibits peaks during the morning (09:00-12:00 hours) and at midnight (21:00-02:00 hours), which are connected to local industrial stack emissions.

The $PM_1$ particle number concentration ranges from 408 to 29,845 particles/$cm^3$ (11319 ± 5552). Elevated particle number concentrations are commonly linked to local burning incidents. The particle concentration sees a rise in the evening (at 06:00 PM) and peaks at midnight, implying an increase in residential burning activity and traffic exhaust emissions. These activities likely contribute to the decrease in the geometric mean diameter (GMD) of the PNSD, which is around 47 nm. However, this value increases to nearly 87 nm, as shown in Fig. 3(t), indicating the organic aerosol's nighttime aging. Fig. 3(y) depicts that the hourly averaged mean diurnal GMD of PVSD varies from about 274 to 324 nm, with a mean value of 309.1 ± 33.1 nm. This average is similar to the higher-end particle size of 200 nm hygroscopicity measurement used in this study. Therefore, the ACSM bulk aerosol composition is the most appropriate option for discussing the hygroscopicity of these particles.

The $PM_1$ concentration, also known as hourly time-resolved NR-$PM_1$, ranged from 9.0 to 357.9 µg/$m^3$ with an average of 81.2 ± 56.6 µg/$m^3$. This range is consistent with the 12.7-392 µg/$m^3$ (NR-$PM_1$) boundary previously reported by Gani et al. (2019) at the same sampling location. Prakash et al. (2018) found that $PM_1$ mass concentration accounts for 83% of $PM_{2.5}$, indicating the prevalence of combustion-based particles. Additionally,

**Supprimé:** suggest …the possibility presence …f daytime photo-oxidation processes according to research carried out by (…elson et al.,…(2023). Fig. S6 displays the variation ofThe…wind speed (…S)…and wind direction (…D, ranging ) varied …rom 0.0 to 5.6 (with an average of 1.0 ± 1.0) m/s and 4.0 to 345.7 (with an average of 197.1 ± 84.4) degrees from the North, respectively, as shown in Fig. S6… The majorityPredominant…of wind directions were in the WNW-WSW and E-ESE direction. These patterns indicatesuggest…that the air quality in Delhi remainedatmosphere remains…relatively stagnant during…hroughout the study period,… and t…he measured aerosols are likely to be a result ofrepresent…local emissions and local …erosol chemistry in Delhi …

**Supprimé:** Additionally… ambient trace gases NOx and CO demonstrate notableexhibit significant…variability throughout the sampling period… peaking fromduring…local burning activities. During intense biomass burning activities, A…mbient NOx levels reach a maximum of 421.2 ppb (58.4 61.9) during intense biomass burning activities… CO concentrations also reach maximum levelspeak…during similar periods as NOx, and…varying from 0.0 to 7.66 ppm (0.58 ± 0.79), as illustratedshown…in Fig. S5. The time-specific changes in the levels diurnal variation …f these trace gases are illustratedis…presented …n Fig. 3 (f, g, h, and i).,…The graph indicates two crestswith two peaks…(06:00-08:00 and 17:00-20:00 hours), which are attributedassociated…with morning …o local biomass/trash burning emissions that happen in the morning and heavy traffic during nighttime traffic …ush hours. ConverselyIn contrast… $SO_2$ demonstrates a distinct patternfollows a different trend …

**Supprimé:** d

**Supprimé:** ynamic variations…ranging from 0.46 to 9.55 ppb (4.41 ± 1.20). Notably, it exhibits and showing …eaks during in …he morning (09:00-12:00 hours) and at midnight (21:00-02:00 hours), which are connected to associated with the …

**Supprimé:** High…particle number concentrations are commonly linked totypically associated with…local burning incidentsevents… The particle concentration sees increa… riseses…in the evening (at 0618…00 hours…M) and peaksreaches its maximum value…at midnight, implying an increase insuggesting the resumption of…residential burning activity and traffic exhaust emissions. These activities likely contribute to the decrease in thelower…geometric mean diameter (GMD) of the particle number size distribution (…NSD,,…which is aroundapproximately…47 nm)…,…However, this valuewhich…increases to nearly 87 nm, as shown in Fig. 3(t), indicating nighttime aging of …he organic aerosol's nighttime aging.…Fig. 3(y) depicts that tT…e hourly averaged mean diurnal GMD of PVSD varies from aboutpproximately…274 to 324 nm (Fig. 3(y))… with a mean value of 309.1 ± 33.1 nm.,…This average is similar which is close …o theis…study's …igher-end particle size …

**Mis en forme** …

**Supprimé:** hourly time-resolved NR-$PM_1$ (say hereafter $PM_1$) concentration varied…from 9.0 to 357.9 µg/$m^3$ ,…ith an average ofing…81.2 ± 56.6 µg/$m^3$. This range is consistent withobservation lies well within the boundary of…the 12.7-392 µg/$m^3$ (NR-$PM_1$) boundary previously,…reported by Gani et al. (2019) for…t the same sampling locationsite… Prakash et al. (2018) foundreported…that $PM_1$ mass concentration accounts foris…83% of $PM_{2.5}$, indicating …

we observed a high correlation ($r^2$ = 0.83, p<0.05) between $PM_1$ measured by ACSM and MPSS, assuming an effective aerosol density of 1.6 g/cm$^3$ (refer to Fig. S4). The OA ranged from 1 and 293 (46.5 ± 39.6) µg/m$^3$, with $PM_1$ being the predominant fraction. These findings are consistent with the range of 53.3 to 166 (112) µg/m$^3$ observed during the winter months (December-February) at the same location (Gani et al., 2019). However, the decrease in average OA concentration during the measuring period of February-March can be explained by the reduction in aerosol loading after its peak in December-January (Gupta and Mandariya, 2013). The campaign average fractional contribution of OA to $PM_1$ was 56%, with a range of 1 to 84%. This high OA concentration in fine particulate matter ($PM_1$) aligns with findings from prior studies in the IGP, including those conducted by Chakraborty et al. (2016a), Gani et al. (2019), and Mandariya et al. (2019), as well as those conducted worldwide, such as by Jimenez et al. (2009) and Zhang et al. (2007). Peak OA mass concentrations were observed between 9:00 PM and 11:00 PM (figure 2(k)), which is in line with observations made at the same site by Gani et al. (2019) and Rai et al. (2020). The average mass concentration of $NO_3$ during the campaign was 10.1 ± 7.0 µg/m$^3$, exhibiting diurnal variation with distinct peaks in the morning and at midnight (Fig. 3(l)). Additionally, $SO_4$ demonstrated a slight enhancement at 08:00 hr, and its concentration remained relatively stable from noon to 17:00 hr (Fig. 3(m)). Conversely, Cl experienced significant fluctuations, ranging from 0.13 to 77.83 µg/m$^3$, with higher concentrations of Cl occurring episodically throughout the campaign. The Cl concentration aligns with Gani et al. (2019)'s previously reported value of 0.1-66.6 µg/m$^3$ at the same location. Fig. 2(g and h) illustrates the temporal variation of various OA factors. The mass concentration of BBOA peaks during the nighttime and morning hours (Fig. 3(r)). On the other hand, LO-OOA exhibits a peak in the morning and remains relatively stable at noontime, indicating a steady formation. Meanwhile, MO-OOA exhibited a slight rise around midday, suggesting daytime photooxidation formation (Mandariya et al., 2019; Sun et al., 2016). During the sampling period, oxygenated organic aerosol (OOA) comprised the majority of OA. The BBOA mass concentration during H-BB events varied dynamically, ranging from 16.3 to 134.7 µg/m$^3$, with an average of 50.7 ± 24.0 µg/m$^3$. Concurrently, these events displayed higher levels of HOA, ranging from 9.6 to 109.4 µg/m$^3$, indicating a likely similarity in the sources of HOA during this particular incident. However, during H-HOA events, concentration of HOA were higher, ranging from 4.8 to 58.9 µg/m$^3$, although these amounts were notably lower than those observed during H-BB events. Nonetheless, the fractional mass contribution of HOA to OA was the largest of all OA categories. Additionally, during H-Cl events, there were increased concentrations of both primary organic aerosol HOA and BBOA. BBOA made up about 40.0%, 21.1%, 32.5%, and 13.1% to OA during H-BB, H-HOA, H-Cl, and relatively clean events, respectively, indicating varied sources of BBOA. Furthermore, the average

**Supprimé:** that ACSM measured $PM_1$ was…highly…correlationed…($r^2$ = 0.83, p<0.05) with…etween MPSS measured …$M_1$ measured by ACSM and MPSS,,…assuming an effective aerosol density of 1.6 g/cm$^3$ (refer to Fig. S42…. The OA ranged frombetween…1 and 293 (46.5 ± 39.6) µg/m$^3$, …ith the predominant fraction of …$M_1$ being the predominant fraction.,…These findings are consistent with the range of 53.3 to 166 (112) µg/m$^3$ observed during the winter months (December-February) at the same locationsite…(Gani et al., 2019). However, the decrease inlower…average OA concentration duringcould be explained by…the measuring period of February-March can explained by the reduction in aerosol loading , as aerosol loading starts decreasing in February …fter reaching …ts peak in December-January (Gupta and Mandariya, 2013). The campaign average fractional contribution of OA to $PM_1$ was 56%, with a range of ranging from … to 84%. This high OA concentrationtribution…in fine particulate matter ($PM_1$) aligni ...

**Supprimé:** c

**Supprimé:** onsistent with other studies conducted in IGP

**Code de champ modifié**

**Supprimé:** (

**Mis en forme :** Français (France)

**Supprimé:** ,…(2016a),;…Gani et al.,…(2019),;…and Mandariya et al.,…(2019), as well as those conducted and…worldwide, such as by (…imenez et al.,…(2009) and;…Zhang et al.,…(2007). Peaked…OA mass concentrations were observednoted…between 921…00 PM and -…123…00 PMhr…(figure 2(k)), which is in line with observations made consistent with previous studies conducted at the samecurrent…site by (…ani et al.,…(2019);…and Rai et al.,…(2020). The Campaign …verage mass concentration of $NO_3$ during the campaign was 10.1 ± 7.0 µg/m$^3$, exhibitingand showed…diurnal variation with distinct a peaks in the morning and at midnight (Fig. 3(l)). AdditionallyBesides… $SO_4$ demonstrated ashowed …slight enhancement at 08:00 hr, and its concentration remained relatively stablenearly constant…from noon to 17:00 hr (Fig. 3(m)). Conversely However… Cl experienced significant fluctuations, ranging from varied between ….13 to 77.83 µg/m$^3$, withand…higher concentrations of Cl occurring episodicallywere found episodic…throughout the campaign. The $Cl^-$…concentration aligns with Gani et al. (2019)'s was found consistent with Gani et al., 2019's …reviously reported value of 0.1-66.6 µg/m$^3$ at the same locationat the same site.… Fig. 2(g and h) illustrates T…he temporal variation of various OA factors. The mass concentration of is presented in Fig. 2(g and h). Biomass burning organic aerosol (…BOA)…mass concentration …eaks during the nighttime and morning hours ((…ig. 3(r)))… On the other hand, Low-volatility oxygenated organic aerosol (…O-OOA)…exhibits a peak in the morning and remains relatively stableconstant…at noontime, indicatingsuggesting…a steady formation. Meanwhile, moderately oxygenated organic aerosol (…O-OOA)…exhibited shows … slight riseincrease…around middaynoontime… suggestingindicating…daytime photooxidation formation through…daytime photooxidation (Mandariya et al., 2019; Sun et al., 2016). During the "ITEM-1", "itemData" : { "DOI" : "10.5194/acp-16-8309-2016", "ISSN" : "16807324", "abstract" : "<p>Winter has the worst air pollution of the year in the megacity of Beijing. Despite extensive winter studies in recent years, our ...

contribution of H-HOA was the highest during the H-HOA event, at 41.6%. During the H-Cl event, Cl's contribution to the fractional mass in $PM_1$ peaked up to 44.9%, which was higher than the contributions of 21.2% in H-BB events and 7.3% in H-HOA events.

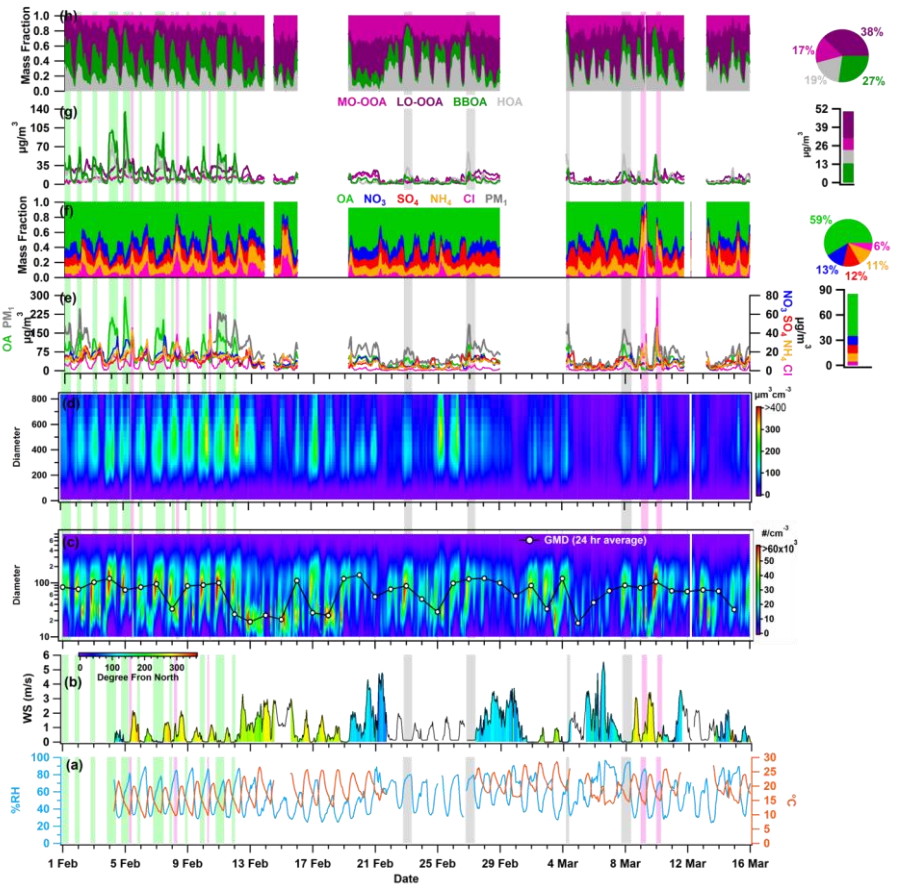


**Figure 2: Temporal variability of ambient (a) relative humidity (RH), temperature (T), (b) wind speed (WS), wind direction (WD), (c) particle number-size distribution (PNSD), 24-average geometric mean diameter (GMD), (d) particle volume-size distribution (PVSD), (e) particulate matter ($PM_1$), organic aerosol (OA), nitrate ($NO_3$), sulfate ($SO_4$), ammonium ($NH_4$), chloride (Cl), (f) fractional contribution of OA, $NO_3$, $SO_4$, $NH_4$, and Cl in $PM_1$, (g) more oxidized-oxygenated OA (MO-OOA), less oxidized-oxygenated OA (LO-OOA), biomass burning OA (BBOA), hydrocarbon like-OA (HOA), and (h) fractional contribution of MO-OOA, LO-OOA, BBOA, and HOA in OA. The pie chart sub-plot represents the overall average contribution of species, and the bar sub-plot represents the overall campaign average**

**Supprimé:** event, HOA's average contribution
**Supprimé:** among all
**Supprimé:** s
**Supprimé:** Additionally, Cl's
**Supprimé:** contribution
**Supprimé:** reached up to
**Supprimé:** during the H-Cl event, in contrast to

value of different species. All other species are represented with specific color coding mentioned in legends. The light green, grey, and pink color shaded vertical line indicates the high-BBOA (H-BB), high-HOA (H-HOA), and high-Cl (H-Cl) events, respectively. The discontinuity in the data points marks the missing data or non-sampling time.

Supprimé: pink, and

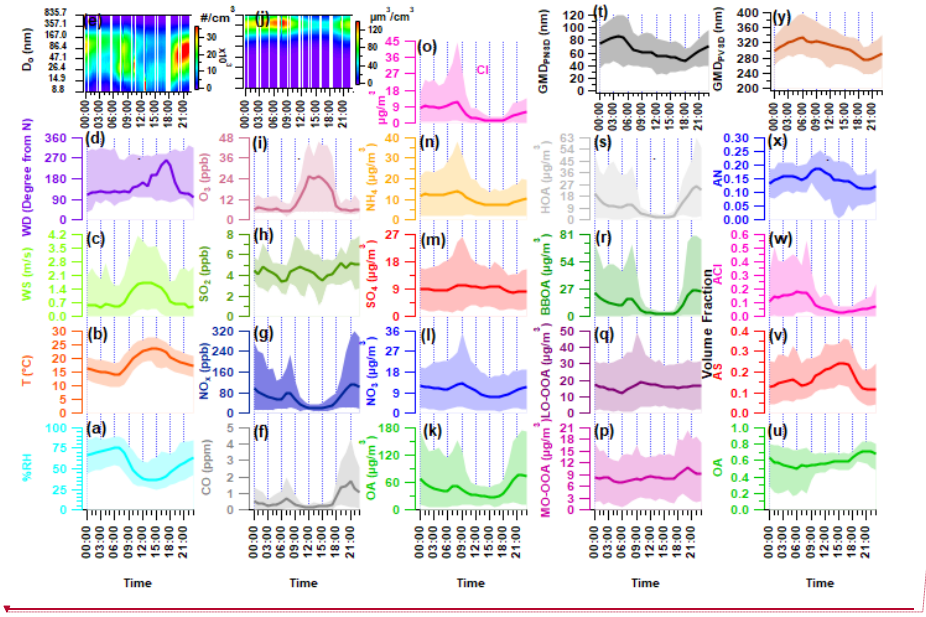


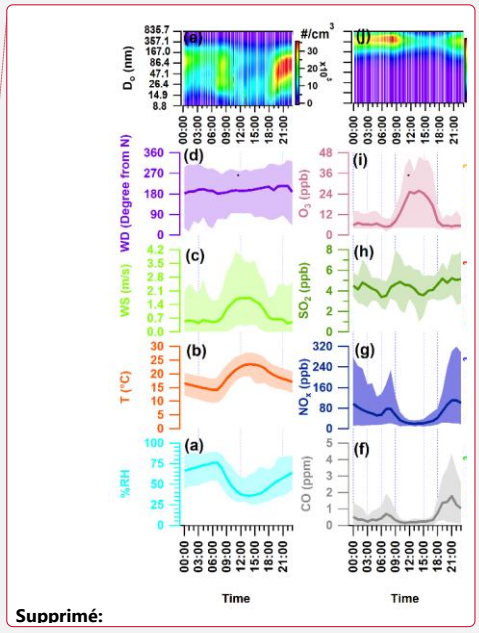


Supprimé:

Figure 3: Diurnal variation of ambient meteorological parameters (a) % ambient relative humidity (RH), (b) temperature (T), (c) wind speed (WS), (d) wind direction (WD), and (e) particle number size distribution (PNSD), mass concentration of ambient trace gases (f) carbon mono-oxide (CO), (g) nitrogen oxides (NOx), (h) sulfur dioxide ($SO_2$), and (i) ozone ($O_3$), (j) particle volume size distribution (PVSD), mass concentration of aerosol constituents (k) organic aerosol (OA), (l) nitrate ($NO_3$), (m) sulfate ($SO_4$), (n) ammonia ($NH_4$), and (o) chloride (Cl), mass concentration of organic aerosol species (p) more oxidized-oxygenated OA (MO-OOA), (q) less oxidized-oxygenated OA (LO-OOA), (r) biomass burning OA (BBOA), and (s) hydrocarbon like-OA (HOA), (t) geometric mean diameter of particle number size distribution ($GMD_{PNSD}$) and volume fractional contribution of (u) organic aerosol (OA), (v) ammonium sulfate (AS), (w) ammonium chloride (ACl), and (x) ammonium nitrate (AN) in $PM_1$, and (y) geometric mean diameter of particle volume size distribution ($GMD_{PVSD}$). Upper and lower boundary of shaded area represents the 95$^{th}$ and 5$^{th}$ percentile values of respective species.

### 3.2 Hygroscopicity of Nucleation, Aitken, and Accumulation Mode Particles

### 3.2.1 Temporal variability

Fig. 4 displays the hourly averaged dynamic variability of $HGF_{90\%}$ and $\kappa_{H\text{-}TDMA\_90\%}$ (kappa) for aerosol particles in the Nucleation, Aitken, and Accumulation modes at 90% ambient relative humidity. The hygroscopic growth factors of particles sized at 20 ($HGF_{90\%\_20nm}$), 50 ($HGF_{90\%\_50nm}$), 100 ($HGF_{90\%\_100nm}$), 150 ($HGF_{90\%\_150nm}$), and 200 nm ($HGF_{90\%\_200nm}$) varied between 1.00-1.41, 1.05-1.39, 1.11-1.49, 1.12-1.63, and 1.12-1.79. The averaged hygroscopic growth factors of the 20, 50, 100, 150, and 200 nm aerosol particles were 1.14 ± 0.09 (average ± standard deviation), 1.16 ± 0.06, 1.27 ± 0.07, 1.35 ± 0.09, and 1.41 ± 0.09, respectively. These values indicate statistical significance ($p<0.05$) between the different hygroscopic growth factors. Moreover, the hygroscopicity values ($\kappa_{20nm\_90\%}$ and $\kappa_{50nm\_90\%}$) of the aerosol particles were found to range between 0.00-0.11 and 0.02-0.25 for the 20 nm and 50 nm particle sizes, respectively, with an average of 0.03 ± 0.02 and 0.09 ± 0.03. Nucleation mode particles, consisting mainly of monomodal GF-PDF (Fig. 4(a)), consisted of approximately 74 ± 24% nearly hydrophobic particles (HGF <1.2). However, this percentage increased to 100% and was associated with nighttime local burning activities, as demonstrated in Fig. 4(a). The nucleation mode particles ($\kappa_{20nm\_90\%}$) exhibited significantly ($p<0.05$) lower hygroscopicity than the Aitken mode particles ($\kappa_{50nm\_90\%}$). Hong et al. (2015) found that nucleation mode particles have higher susceptibility to condensable vapors such as newly-emitted VOCs, $H_2SO_4$ and HCl. Nevertheless, the study at hand did not measure these substances. The $\kappa$ value of Aitken-sized particles was comparable to the 0.24 ± 0.08 of 52.6 ± 6.9 size particles reported by Gunthe et al. (2011) for Beijing, like Delhi, is one of the most polluted urban area. Gunthe et al. (2011) conducted this study on CCN at supersaturation levels, justifying the comparison. The campaign average hygroscopicity parameter (kappa, $\kappa_{90\%}$) increased significantly ($p<0.05$) with particle size, attributed to the Kelvin effect (Wang et al., 2018a). In the accumulation size range of 100, 150, and 200 nm, $\kappa_{90\%}$ increased to approximately 0.56. The mean values for $\kappa_{100nm\_90\%}$, $\kappa_{150nm\_90\%}$, and $\kappa_{200nm\_90\%}$ were 0.14 ± 0.04, 0.18 ± 0.06, and 0.22 ± 0.07, respectively. The range for $\kappa_{200nm\_90\%}$ was between 0.05 and 0.56. Similar variations of $\kappa$ with particle size have been observed globally (Cerully et al., 2015; Enroth et al., 2018; Fan et al., 2020; Kawana et al., 2016; Kim et al., 2020; Kitamori et al., 2009; Ogawa et al., 2016; Sjogren et al., 2012; Wang et al., 2018a), including in Kanpur, India, situated in the center of the IGP (Mandariya et al., 2020a). These variations have been attributed to the prevalent increase in inorganic to organic aerosol fraction in particles with size increment. Furthermore, Arub et al. (2020) reported that $\kappa_{H\text{-}TDMA\_90\%}$ was approximately in the range of 0.13-0.77 for $PM_1$ in Delhi, without considering BC. However, their theoretical prediction of particles' hygroscopicity took into account a particle's chemical composition, leading to more precise results. Arub et al. (2020) thus provided a theoretical prediction of particles'

**Supprimé:** shows…the dynamic variability in the …ourly averaged dynamic variability of $HGF_{90\%}$ and hygroscopicity parameter (…$_{H\text{-}TDMA\_90\%}$,…(kappa) for aerosol particles in theof…Nucleation, Aitken, and Accumulation modes aerosol particles …t 90% ambient relative humidity. The hygroscopic growth factors of particles sized at 20 ($HGF_{90\%\_20nm}$), 50 ($HGF_{90\%\_50nm}$), 100 ($HGF_{90\%\_100nm}$), 150 ($HGF_{90\%\_150nm}$), and 200 nm ($HGF_{90\%\_200nm}$) size particles …aried between 1.00-1.41, 1.05-1.39, 1.11-1.49, 1.12-1.63, and 1.12-1.79. The with an …veraged hygroscopic growth factors of the 20, 50, 100, 150, and 200 nm aerosol particles were 1.14 ± 0.09 (average ± standard deviation), 1.16 ± 0.06, 1.27 ± 0.07, 1.35 ± 0.09, and 1.41 ± 0.09, respectively. These values indicate mean hygroscopic growth factors were noted as …tatistical significancely…($p<0.05$) between the different hygroscopic growth factorsfrom each other… MoreoverIn addition… the hygroscopicity values ($\kappa_{20nm\_90\%}$ and $\kappa_{50nm\_90\%}$) of the aerosol particles were found to range 20 and 50 nm aerosol particles varied …etween 0.00-0.11 and 0.02-0.25 for the 20 nm and 50 nm particle sizes,,…respectively, with an average of 0.03 ± 0.02 and 0.09 ± 0.03, respectively… Nucleation mode particles, consisting were observed,…mainly of monomodal GF-PDF (Fig. 4(a)), conmpri…istedng…of approximately nearly …4 ± 24% nearly hydrophobic particles (HGF <1.2). However, this percentage increasedcontribution was raised…to 100% and , which…was associatedobserved to have a good association…with night-…ime local burning activities, as shown…emonstrated in the …ig. 4(a). The nucleation mode particles ($\kappa_{20nm\_90\%}$) exhibitedshowed significantly ($p<0.05$) lower hygroscopicity than the Aitken mode particles ($\kappa_{50nm\_90\%}$). Hong et al. (2015) foundreported…that nucleation mode particles are …ave higher susceptibility more sensitive …o condensable vapors such aslike…newly-emittedfresh…VOCs, $H_2SO_4$ and HCl. NeverthelessHowever… the present …tudy at hand did not measure these substancesspecies… The $\kappa$ value of Aitken-sized particles wasere…comparable to thewith…0.24 ± 0.08 of 52.6 ± 6.9 size particles reported by Gunthe et al. (2011) for Beijing, like Delhi,…Beijing …s also …ne of the most polluted urban arealocations like Delhi,… which could justify the comparison. However, …ADDIN CSL_CITATION { "citationItems" : [ { "id" : "ITEM-1", "itemData" : { "DOI" : "10.5194/acp-11-11023-2011", "ISSN" : "1680-7324", "abstract" : "Abstract. Atmospheric aerosol particles serving as cloud condensation nuclei (CCN) are key elements of the

**Déplacé (insertion) [2]**

**Mis en forme**

**Code de champ modifié**

**Supprimé:** demonstrated…in Kanpur, India, situated at…n the center of the IGP, India…(Mandariya et al., 2020a). These variations have beenand worldwide studies

**Déplacé vers le haut [2]:** (Cerully et al., 2015; Enroth et al., 2018; Fan et al., 2020; Kawana et al., 2016; Kim et al., 2020; Kitamori et al., 2009; Ogawa et al., 2016; Sjogren et al., 2012; Wang et al., 2018a)

**Supprimé:** . Moreover, this was…attributed to the prevalentdominant…increasement…in inorganic to organicOA…aerosol fraction in particles with size increment in size… Furthermore, Arub et al. (2020) reported that $\kappa_{H\text{-}TDMA\_90\%}$ was found …pproximately in the range of 0.13-0.77 for,…$PM_1$reported…inby Arub et al. (2020) at…Delhi, for $PM_1$ …ithout considering BC. However, their theoretical

**Mis en forme**

hygroscopicity by considering a particle's chemical composition. A 10% in $\kappa$ calculation was observed when considering BC in the aerosol chemical composition. Additionally, the $\kappa_{H\text{-}TDMA\_90\%}$ measured in this study aligned with the global average value of 0.27 ± 0.21 for continental aerosols (Petters and Kreidenweis, 2007; Pringle et al., 2010). Subsequent sections will discuss the impact of a particle's chemical composition, local meteorology, and air mass trajectories on $\kappa_{H\text{-}TDMA\_90\%}$ for accumulation mode particles.

**Supprimé:** theoretically predicted particles'

**Supprimé:** They found a decrease in $\kappa$ calculation by

**Supprimé:** when BC

**Supprimé:** ed

**Supprimé:** lso

**Supprimé:** e

**Supprimé:** current

**Supprimé:** were found in line

**Supprimé:** Further, to understand

**Supprimé:** discussed in subsequent sections

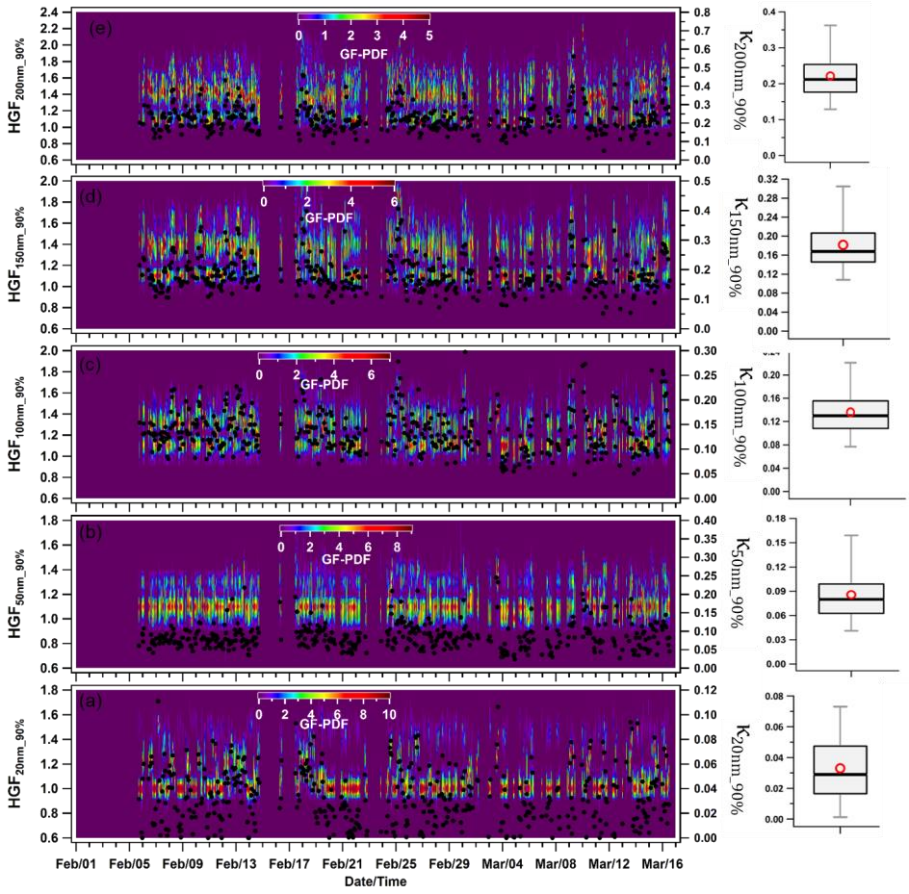


**Figure 4: Temporal variability in hygroscopicity parameter kappa ($\kappa$) of nucleation mode particles (a) 20 nm ($\kappa_{20nm\_90\%}$), Aitken mode particles (b) 50 nm ($\kappa_{50nm\_90\%}$), and Accumulation mode particles (c) 100 nm ($\kappa_{100nm\_90\%}$), (d) 150 nm ($\kappa_{150nm\_90\%}$), and (e) 200 nm ($\kappa_{200nm\_90\%}$). The box plots represent the variability in the hygroscopicity of**

**respective sizes of particles in which low and high whisker traces represent the 5 and 95 percentile, respectively. The red marker indicates the average of the data, whereas the upper and lower sides of the boxes indicate the 75 and 25 percentile of the data, respectively.**

### 3.2.2 Diurnal variability

The diurnal variation in $\kappa_{H\text{-}TDMA\_90\%}$ differed for nucleation ($\kappa_{20nm\_90\%}$), Aitken ($\kappa_{50nm\_90\%}$), and Accumulation ($\kappa_{100nm\_90\%}$, $\kappa_{150nm\_90\%}$, and $\kappa_{200nm\_90\%}$) mode particles. Fig. 5 illustrates the hourly-resolved average $\kappa$ for each particle size, showing a diel trend. The larger particles displayed higher $\kappa$ values than the smaller ones, consistent with trends observed in Kanpur, India (Mandariya et al., 2020a) and other locations worldwide (Fan et al., 2020; Hong et al., 2015). Overall, all particle sizes exhibited a "late-night hump" (02:00-05:00 hr) in $\kappa_{H\text{-}TDMA\_90\%}$. Only $\kappa_{20nm\_90\%}$ displayed a diurnal variation with two peaks: one occurring late at night (02:00-04:00 hr) and the other at noon (14:00-16:00 hr). Additionally, two valleys were observed during the morning (07:00-10:00 hr) and night (19:00-22:00 hr), which indicate the strong influence of local burning and traffic activities (Pringle et al., 2010). Furthermore, nucleation-sized particles were potentially contributed by nearly hydrophobic particles (HGF<1.2) from evening to midnight. Mono-modal GF-PDF was exhibited around a unit hygroscopic growth factor, potentially suggesting the presence of locally-emitted particles. The 20 nm particles are of sufficient small size to be classified as nucleation mode particles. Similar diurnal trends of Nucleation and Aitken mode particles have been observed by Achtert et al. (2009), who attributed the lower values to the emission of hydrophobic aerosol particles during the local burning emissions. The daytime hump in aerosol particle composition can be attributed to the intensity of the photochemical oxidation process, resulting in the amplification of more oxidized species. Moreover, the gaseous condensation of $H_2SO_4$, $HNO_3$, and VOCs predominantly controls their chemical makeup (Hong et al., 2015). The variability of $\kappa_{H\text{-}TDMA\_90\%}$ can be addressed by taking into account the chemical composition of the aerosol. Although $\kappa_{50nm\_90\%}$ exhibited less variation, it follows a diurnal pattern similar to $\kappa_{20nm\_90\%}$. Furthermore, when the dry size of the aerosol particles increased to the accumulated mode, the diurnal variation shifted towards nearly constant for the rest of the day. Hong et al. (2018) found no discernible diurnal variation of 100- and 150-nm particles of organic-dominated aerosols in China's Pearl River Delta region.

Furthermore, the diurnal cycles of aerosol physicochemical properties also reflect the dynamic diurnal variation in the planetary boundary layer (PBL), leading to particle accumulation during the night. The study only addressed trend variability using bulk-aerosol composition, as size-resolved chemical composition was not quantified. However, the daily average aerosol PNSD ranged from 18.0-140.0 nm, with a mean of 73.1 ± 33.8 nm. The shift

**Supprimé:** bility…in $\kappa_{H\text{-}TDMA\_90\%}$ was found differednt…for nucleation ($\kappa_{20nm\_90\%}$), Aitken ($\kappa_{50nm\_90\%}$), and and Accumulation ($\kappa_{100nm\_90\%}$, $\kappa_{150nm\_90\%}$, and $\kappa_{200nm\_90\%}$) mode particles. Fig. 5 illustrates the hourly-resolveddisplayed a diel variation of an…average of hourly-resolved ... for each particle size, showing a diel trend. The largerbigger size…particles displayedexhibited…higher values of ... values than the smaller onessize particles… consistent with trends observed inwhich is a similar trend reported at…Kanpur, India (Mandariya et al., 2020a) and other locations worldwide locations…(Fan et al., 2020; Hong et al., 2015). OverallIn general… it was observed that …ll size particles…sizes exhibited a "late-night hump" (02:00-05:00 hr) in $\kappa_{H\text{-}TDMA\_90\%}$. Besides, o…nly $\kappa_{20nm\_90\%}$ displayedemonstrated…a clear …iurnal two peaks:,…one occurring late at night (02:00-04:00 hr) and the other in…t noontime…(14:00-16:00 hr).,…Additionallyand… two valleys were observed during the morning (07:00-10:00 hr) and night (19:00-22:00 hr), which indicate . These valleys reflects …he strong influence impacts …f local burning and traffic activities (Pringle et al., 2010). FurthermoreIn addition… nucleation- …ized particles were potentially contributed by nearly hydrophobic particles (HGF<1.2) from evening to midnight. They showed m…ono-modal GF-PDF was exhibited around a unit hygroscopic growth factor, potentiallyssibly…suggesting the presence of indicating…locally- …mittedssion…generated …articles. 20 nm particles are of sufficient small size to be classified assmall enough and lie on the boundary of ...

**Déplacé vers le bas [3]:** Achtert et al. (2009)

**Supprimé:** reported a …s ...

**Déplacé (insertion) [3]**

**Supprimé:** D…aytime hump in aerosol particle composition can beis…attributed to the intensitye…of the photochemical oxidation process, resulting inwhich causes…the amplificationenhancement …of more oxidized species on the aerosol particle… MoreoverFurthermore… their chemical composition is dominantly controlled by …he gaseous condensation of $H_2SO_4$, $HNO_3$, and VOCs predominantly controls their chemical makeup …ADDIN CSL_CITATION { "citationItems" : [ { "id" : "ITEM-1", "itemData" : { "DOI" : "10.5194/acp-15-11999-2015", "ISSN" : "16807324", "abstract" : "Measurements of the hygroscopicity of 15-145 nm particles in a boreal forest environment were conducted using two Hygroscopicity Tandem Differential Mobility Analyzer (HTDMA) systems during the Pan-European Gas-Aerosols-climate interaction Study (PEGASOS) campaign in spring 2013. Measurements of the chemical composition of non-size segregated particles were also performed using a high-resolution aerosol mass spectrometer (HR-AMS) in parallel with hygroscopicity measurements. On average, the hygroscopic growth factor (HGF) of particles was observed to increase from the morning until afternoon. In case of accumulation mode particles, the main reasons for this behavior were increases in the ratio of sulfate to organic matter and oxidation level (O : C ratio) of the organic matte ...

**Supprimé:** that …eadings…to particlethe…accumulation of particles …uring the night-time… Although t…heis…study only addressed trend variability using bulk-aerosoldid not quantify size-resolved chemical …composition, as size-resolved chemical composition was not quantifiedso, this study used bulk-aerosol composition to address the trend variability only… However, the daily average aerosol PNSD ranged fromvaried between ...

in PVSD mode occurred in the 300-600 nm. Range, making it appropriate to analyze the $\kappa_{200nm\_90\%}$ variation in association with the bulk chemical properties of aerosols. Fan et al. (2020) demonstrated in Fig. 3 (r, s t, u, and v) that the increase in the ratio of inorganic volume fraction to OA volume fractions is responsible for the peak in hygroscopicity observed in the early morning hours. Additionally, in the winter, during mid-night and early morning, water-soluble organic and inorganic gases undergo partitioning and/or coagulation/condensation on the surface of pre-existing particles. Furthermore, at high RH and lower temperatures, primary and secondary, less-oxidized organic aerosols engage in the aging process. This leads to improved oxidation through aqueous/heterogeneous reactions, thereby increasing the hygroscopicity of the particles (Jimenez et al., 2009; Wu et al., 2016). Similar findings were reported by Fan et al. (2020) for winter in urban Beijing. They have attributed this to the increase in hygroscopic particles due to the aqueous-oxidation and/or condensation process on the pre-existing particles. Generally, stronger noontime solar radiation promotes more intense photooxidation processes. The process promotes the distribution of fairly more oxidized and less volatile organics on the surface of particles, thus augmenting the hygroscopic nature of particles that belong to the accumulation mode (Duplissy et al., 2011; Massoli et al., 2010; Tritscher et al., 2011). The $\kappa_{H\text{-}TDMA\_90\%}$ exhibited a noontime flattening pattern, which was due to a combination of the positive and negative effects resulting from an increase in the volume fraction of OA and more hygroscopic ammonium sulfate and a decrease in ACl, and AN's volume fraction. A potential factor that modulates the hygroscopicity of accumulation mode particles is the lower volume fraction contribution of highly volatile ACl. This correlation is strongly supported by the $\kappa_{H\text{-}TDMA\_90\%}$ and the volume fraction of ACl ($\varepsilon_{ACl}$) in the corresponding size particles.

**Supprimé:** And, the mode of…PVSD mode occurred in the changed approximately around …

**Mis en forme :** Indice

**Supprimé:** Therefore, it could be an excellent approximation to discuss $\kappa_{200nm\_90\%}$ variability with aerosol's bulk chemical properties.…Fan et al. (2020) demonstrated in Fig. 3 (r, s t, u, and v) that the increase The midnight to early morning hump in hygroscopicity of accumulation mode particles can be attributed to the high rise …n the ratio of inorganic volume fraction to OA volume fractions is responsible for the peak in hygroscopicity observed in the early morning hours. (Fan et al., 2020), as illustrated in figure 2 (r, s t, u, and v).…Additionally, in the winterMoreover,…during mid-night and early morning in the winter… water-soluble organic and inorganic gases undergoare…partitioninged…and/or coagulationed…condensationed…on the surface of the…pre-existing particles. Furthermore, at in the presence of …igh RH and lower temperatures, primary and secondary, less-oxidized organic aerosols engageparticipated…in the aging process.,…Thiswhich…leads to improvedenhancement their…oxidation throughvia…aqueous/heterogeneous reactions, thereby according to it …ncreasinge…the particle's hygroscopicity of the particles (Jimenez et al., 2009; Wu et al., 2016). Similar findingsresults…were reportedobserved…by Fan et al. (2020) forduring…winter in urban Beijing.,…and t…hey have attributed this toit with…the increase inenhancement of more…hygroscopic particles due to the aqueous-oxidation and/or condensation process on the pre-existing particles. In g…enerally, higher…tronger noontime solar radiation promotesfavours…more intense photooxidation processes. The process promotesIt…the distribution of fairly supports the partitioning of relatively…more oxidized and less volatile organics on the particulate …urface of particles, thus augmentingenhancing…the hygroscopicity…nature of accumulation mode …articles that belong to the accumulation mode (Duplissy et al., 2011; Massoli et al., 2010; Tritscher et al., 2011). TheHowever, interestingly, we observed a noontime flatten pattern of…$\kappa_{H\text{-}TDMA\_90\%}$,…exhibited a noontime flattening pattern, which was due to a combinationand it could be attributed to the mix…of the positive and negative effects resulting from impact of …n increase enhancement …n the volume fraction of OA and hygroscopic ammonium sulfate and a decrease decrement …n ACl, and AN's volume fraction. A potential factor that modulates the hygroscopicity of accumulation mode particles is the lower volume fraction contribution of highly volatile ACl.Lower volume fractional contribution of highly volatile ACl could be the potential factor that modulates accumulation mode particle's hygroscopicity.…This can be supported by the strong …orrelation is strongly supported by theof…$\kappa_{H\text{-}TDMA\_90\%}$ and the volume fraction of ACl ($\varepsilon_{ACl}$) in the correspondingthat…size particles ($\varepsilon_{ACl}$) …

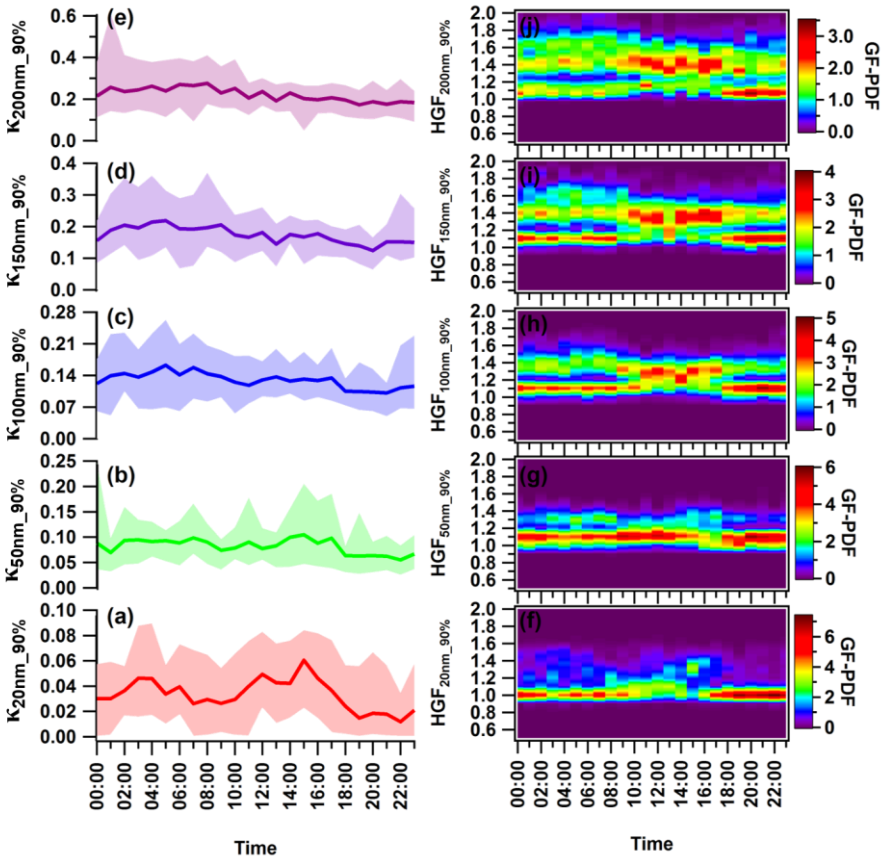


**Figure 5: Diurnal variance in the hygroscopic parameter kappa ($\kappa$) of nucleation mode particles (a) 20 nm ($\kappa_{20nm\_90\%}$), Aitken mode particles (b) 50 nm ($\kappa_{50nm\_90\%}$), and Accumulation mode particles (c) 100 nm ($\kappa_{100nm\_90\%}$), (d) 150 nm ($\kappa_{150nm\_90\%}$), and (e) 200 nm ($\kappa_{200nm\_90\%}$) and hygroscopic growth factor of (f) 20 nm ($HGF_{20nm\_90\%}$), (g) 50 nm ($HGF_{50nm\_90\%}$), (h) 100 nm ($HGF_{200nm\_90\%}$), (i) 150 nm ($HGF_{150nm\_90\%}$), and 200 nm ($\kappa_{200nm\_90\%}$) aerosol particles. The solid line represents diurnal average values, and the upper and lower shaded area represents 95 and 5 percentile values of corresponding average values. Different color coding has been used to represent various size-specific kappa values. The color scale represents the growth factor probability density function of hygroscopic growth factor.**

### 3.2.3 Driving Factor of Hygroscopicity

A correlation analysis was conducted between the measured chemical species and aerosol hygroscopicity to investigate the factors governing aerosol hygroscopicity, as presented in Fig. 6. It was found that organic aerosol

**Supprimé:** arried out
**Supprimé:** explore
**Supprimé:** shown
**Supprimé:** the
**Supprimé:** Organic aerosol
**Supprimé:** observed
**Supprimé:**

negatively affected κ, as evidenced by a negative correlation (Fig. S7(a)). The negative correlation between OA and κ has been noted in India (Bhattu et al., 2016; Mandariya et al., 2020b) and globally (Enroth et al., 2018; Hong et al., 2014; Kawana et al., 2016; Kitamori et al., 2009; Wang et al., 2018a; Wu et al., 2013a). These findings suggest that primary constituents were predominant during high loading and may have been nearly hydrophobic or less hygroscopic. The present study found that a 10% increase in volume of OA in 200 nm aerosol particles led to a 4% reduction in their ability to attract water (hygroscopicity) (Fig. S7(a)). It is noteworthy that ammonium sulfate and nitrate exhibited a weak positive correlation with hygroscopicity (Fig. 7(b and c)). This may be attributed to sulfate and nitrate aerosols dominant in larger particles (>200nm). However, an increase in AS volume by 10% was found to be responsible for a mere 1.6% increase in hygroscopicity. If the aerosol composition had an increased AS contribution, the water-bound capacity of the aerosol was negatively affected (refer to Fig. S8b). Additionally, as shown in Fig. 6(a), there was an increase in the volume fraction of ACl in $PM_1$ with an increase in aerosol hygroscopicity. This strong positive correlation was responsible for a 4.2% increase in kappa over the increment of 10% ACl by volume. This was the highest among all chemical species. Furthermore, ammonium chloride has a greater capacity for water absorption (Chen et al., 2022; Zhao et al., 2020), which is supported by the strong correlation between ALWC and the mass fraction of ACl in $PM_1$ as demonstrated in Fig. 6(b). The increasing fraction of ACl in $PM_1$ may therefore be attributed to the higher water uptake potential of ammonium chloride. This implies that particles with a higher proportion of ammonium chloride absorb more water vapor, resulting in larger hygroscopic aerosol particles. It is evident that the rise in ammonium chloride proportion amplifies aerosol liquid water content, resulting in greater aerosol particle hygroscopicity. A recent study conducted in Delhi by Chen et al. (2022) revealed that the fraction of ammonium chloride in $PM_1$ aerosol increases significantly during higher relative humidity conditions in the winter season. This is due to the co-condensation of semivolatile ammonium chloride with water vapor on particles, leading to enhanced water uptake and severe winter haze in Delhi. The high volume fractions (over 30%) of ACl in atmospheric $PM_1$ were observed sporadically, leading to the conclusion that the high chloride fraction in the particle phase heavily relies on excess ammonia in the atmosphere. These findings suggest that ammonia plays a crucial role in determining chloride partitioning in the particle phase, leading to increased aerosol water content in high relative humidity conditions and lower temperature. The concentration of ACl relies heavily on both RH and temperature.

**Supprimé:** impact…κ, as evidenced explained …y a negative correlation (Fig. S7(a)). This… negative correlation betweenof…OA andwith…κ has been notedis also observed…in India (Bhattu et al., 2016; Mandariya et al., 2020b) and globallyworldwide…(Enroth et al., 2018; Hong et al., 2014; Kawana et al., 2016; Kitamori et al., 2009; Wang et al., 2018a; Wu et al., 2013a). Thei…e findings suggestresult indicates…that primary constituents were OA …uring high loading and may have been, considered…nearly hydrophobic or less hygroscopic. In addition, t…he presentcurrent…study foundobserved…that an…enhancement of …0% increase in volume of OA by volume …n 200 nm aerosol particles led towould be responsible for…a 4% reductiondecrement…in their ability to attract waterits…(hygroscopicity) (Fig. S7(a)). It is noteworthy thatInterestingly,…ammonium sulfate and nitrate exhibited showed … weak positive but poor …orrelation with hygroscopicity (Fig. 7(b and c)). This mayIt could…be attributeddue…to sulfate and nitrate aerosols dominati…tg…inthe…larbig…er particles (>200nm). However, an increase in AS volume by 10% enhancement of AS by volume …as found to be responsible for a merethe enhancement of hygroscopicity only by…1.6% increase in hygroscopicity. If the aerosol composition had an increased AS contribution, theBut if AS contribution increased in the aerosol composition, aerosol…water-bound capacity of the aerosol was negatively affectedimpacted…(refer to Fig. S8b). AdditionallyBesides… as shown in Fig. 6(a), there wasshown…an increaseing…in the volume fraction of ACl in $PM_1$ with an increase in aerosol hygroscopicity.,…and t…his strong positive correlation wasis…responsible for an…enhancement in kappa by ….2% increase in kappa over the increment of 10% ACl by volume.,…Thiswhich…was the highest among all chemical species. Furthermore, ammonium chloride has a greater capacity formore significant…water absorptionuptake potential…(Chen et al., 2022; Zhao et al., 2020), which is supportedcan be justified…by the strongolid…correlation betweenof…aerosol liquid water content (…LWC)…and thewith a…mass fraction of ACl in $PM_1$ as demonstrated shown …

**Mis en forme :** Indice

**Supprimé:** indicates…that particles with a higher proportion ofmore considerable…ammonium chloride absorbfraction uptake…more water vapor, resulting in largerleading to higher…hygroscopic aerosol particles. It is evidentclear…that the riseincreases…in ammonium chloride proportionfraction…enhanced…mplifies aerosol liquid water content, resulting in greater and led to higher hygroscopicity of …aerosol particle hygroscopicitys… A rR…cent study conducted in Delhi by Chen et al. (2022) revealedunveils…that the fraction of ammonium chloride fraction …n $PM_1$ aerosol increases significantlyenormously enhances…during the…higher relative humidity conditions in during …he winter season. due to t…his is due to thee…co-condensation of semivolatile ammonium chloride with water vapor on the…particles, and …eadings…to enhanced water uptake and lead …evere winter haze in Delhi. …he very high volume fractions (over >…0%) of ACl in atmospheric $PM_1$ were observed sporadically, leading to the conclusion that the high chloride fractionepisodic, suggesting a high fraction of Cl…in the particle phase heavily reliesis strongly dependent…on excess ammonia in the atmosphere. These findings suggestresults indicate…that ammonia plays a crucial role in determiningis the controlling factor for…chloride partitioning in the particle phase, leading to increasedresulting in high…aerosol water content …

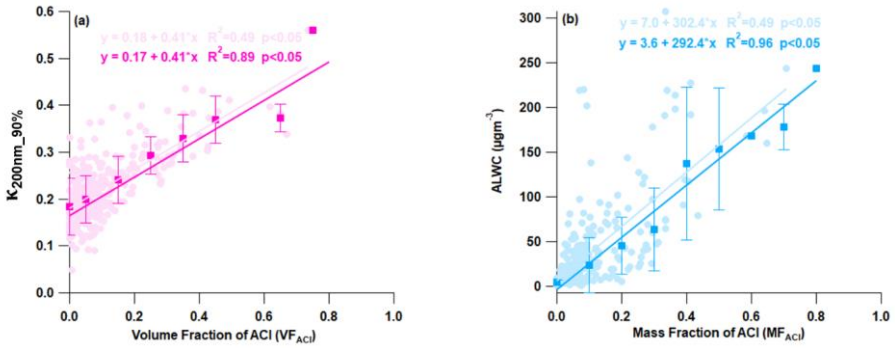


**Figure 6: Correlation plot for (a) $\kappa_{200nm\_90\%}$ vs volume fraction of ammonium chloride aerosol ($VF_{ACl}$) and (b) aerosol liquid water content (ALWC) vs mass fraction of ammonium chloride ($MF_{ACl}$). The solid circle and square marker represent the individual data points and the average of 10% volume and mass fraction increment of ACl data points, respectively. The light and dark color regression lines and equations indicate the overall and average (10% volume and mass fraction increment) correlation, respectively. The error bars indicate the standard deviation of the data points within the 10% mass and volume fractional bins.**

### 3.2.4 Hygroscopicity during high biomass burning (H-BB), high-hydrocarbon like OA (H-HOA), high-Cl (H-Cl), and relatively clean periods

Delhi's atmosphere is a complex mixture of chloride and organic aerosol sources resulting from combustion (including crop residue, agriculture waste, medical waste, municipal waste, plastic, etc.) and industrial activity. To examine the influence of chloride and OA on aerosol hygroscopicity, all episodic events were categorized into three groups. The first group was H-BB events, the second group was H-HOA events, and the third group was H-Cl events. Aerosol chemical composition data was filtered based on hygroscopic parameter data for subsequent analysis. This facilitates the retrieval of data specific to local emissions and atmospheric chemistry, as well as the effects of various potential transported air masses. Extracting any conceivable information pertaining to aerosol sources and transformation processes is valuable in interpreting their impact on aerosol hygroscopicity.

#### 3.2.4.1 High-Cl (H-Cl) events

H-Cl events were selected as they correspond to a significant increase (>20%) in the fractional volume contribution of $NH_4Cl$ ($\varepsilon_{ACl}$) in the $PM_1$ aerosol at the receptor site. During this period, the surface wind mainly came from the west, although it was also influenced by wind from the west-northwest, west-southwest, and southeast, as illustrated in Fig. 7b. The average geometric mean diameter of the PNSD was almost 64 nm,

**Supprimé:** C
**Supprimé:** P
**Supprimé:** array
**Supprimé:** like
**Supprimé:** , burning
**Supprimé:** sources
**Supprimé:** Therefore
**Supprimé:** lassified
**Supprimé:** to investigate the impact of chloride and OA on aerosol hygroscopicity
**Supprimé:** F
**Supprimé:** ,
**Supprimé:** high biomass burning (
**Supprimé:** )
**Supprimé:** ;
**Supprimé:** ,
**Supprimé:** high-hydrocarbon like OA (
**Supprimé:** )
**Supprimé:** ;
**Supprimé:** ,
**Supprimé:** high-Cl (
**Supprimé:** )
**Supprimé:** Further, a
**Supprimé:** ere
**Supprimé:** according to
**Supprimé:** further
**Supprimé:** By performing so, data information that is characteristic of the
**Supprimé:** in question and
**Supprimé:** types can be retrieved
**Supprimé:** It is valuable to extract
**Supprimé:** possible
**Supprimé:** about
**Supprimé:** evaluation to interpret its influence on the aerosol's
**Supprimé:** , representing the substantial loading of ACl on the receptor site,
**Supprimé:** chosen mainly due
**Supprimé:** the
**Supprimé:** jump
**Supprimé:** T
**Supprimé:** observed apparent
**Supprimé:** W-direction, although WNW, WSW, and SE winds also influence the site, as shown
**Supprimé:** GMD
**Supprimé:** nearly

indicating that nearby fresh emission sources impact the particles. In addition, the average concentration of $SO_2$, NOx, and CO concentrations were at 3.6 ppb, 51.9 ppb, and 0.4 ppm, respectively. The potential contributors to BBOA and HOA were from the WNW and SE directions, as demonstrated in the bipolar plot Fig. 7(c & d), and appeared to originate from a local source. Among the inorganic species, ACl displayed a strong correlation with ambient RH, as illustrated in Fig. 7e and f, suggesting that atmospheric gaseous HCl was neutralized by $NH_3$ gas in the presence of atmospheric water content. HCl sources may include coal power plants, solid waste dumping sites with burning trash, and industries in the W-WSW direction (Gani et al., 2019), as depicted in in Fig. 7a. Trash burning in Delhi during winter may potentially dominate atmospheric high Cl events (Shukla et al., 2021; Tobler et al., 2020). In addition, the bipolar plots (Fig. 6(e and f)) indicate that ACl formation occurs under high relative humidity conditions associated with a relatively calm atmosphere, thereby triggering particles hygroscopicity. This hypothesis is supported by the strong correlation between ALWC as discussed in the previous section. Moreover, as shown in Fig. 8d, the GF-PDF of particles of all sizes shows a relatively higher fraction of secondary mode particles contributing. More hygroscopic particles ($HGF_{90\%}$>1.2) accounted for higher percentage of 42%, 47%, 50%, 74%, and 83% in particles ranging from 20nm to 200nm in size, respectively. Therefore, ACl plays a significant role in increasing aerosol hygroscopicity, leading to the formation of fog/haze under higher RH and colder atmospheric conditions.

Gunthe et al. (2021) observed that high local emissions of hydrochloric acid in Delhi during February-March are partitioned into aerosol liquid water under high humidity conditions. This enhances the water uptake capacity of aerosols, sustaining particle hygroscopic growth and resulting in fog/haze formation. Additionally, studies worldwide on size-resolved hygroscopicity have observed Cl to be less than 1%, leading to the omission of ACl as an aerosol constituent in the discussion. The current study did not find a strong correlation between $\kappa$ with AS or AN, which may be due to their association with larger particle sizes. Additionally, ACl may be associated with particles of a comparatively smaller size (≤ 200 nm). Furthermore, in the context of examining the influence of air mass trajectories, we mapped the constituents of aerosols in association with air mass back trajectories using PSCF to determine the potential area source contribution that may be influencing the aerosol evaluation processes, specifically the aerosol's hygroscopicity. However, we did not find any back trajectories that influenced the receptor site, as all trajectory endpoints were observed above the height of the planetary boundary layer.

**Supprimé:** local…fresh emissions…sources impactinfluence…the particles. In addition, the average concentrationmean…of $SO_2$, NOx, and CO concentrations were at 3.6 ppb, 51.9 ppb, and 0.4 ppm, respectively. The potential contributors to BBOA and HOA wereare… potentially contributed …rom the WNW and SE directions, demonstrated explained …n the bipolar plot Fig. 7(c & d), and appearedseem…to originatecome…from a similar …ocal source. Among the inorganic species, ACl displayed a strong correlationobserved excellent association…with ambient RH, as illustratedshown…in Fig. 7e and f, suggesting thatindicating the…atmospheric gaseous HCl was neutralized bywith…$NH_3$ gas in the presence of atmospheric water content. HCl sources may includecould be…coal power plants, trash burnings in …olid waste dumping sites with burning trash, and other …ndustries located …n the W-WSW direction (Gani et al., 2019), as depictedshown…in the map in Fig. 7a. Atmospheric high Cl events are potentially dominated by t…rash burning in Delhi during winter may potentially dominate atmospheric high Cl events (Shukla et al., 2021; Tobler et al., 2020). In additionMoreover… the bipolar plots (f…igure… 6(e and f)) indicatesuggest …that ACl formation occurs under high relative humidityRH…conditions associated with a relatively calm atmosphere, thereby triggering particles'…hygroscopicity. This hypothesis is can be …upported by the strong correlation betweenwith a good association of…aerosol liquid water content (…LWC,)…as discussed in the previous section. MoreoverFurthermore… as shown in Fig. 8d, the GF-PDF of particles of all sizes shows a particle marked relatively more…igher fractionaly… contribution …f secondary mode particles contributingas showed in Fig. 8d… Overall m…ore hygroscopic (HGF90%>1.2) …

**Mis en forme :** Indice

**Supprimé:** were marked by…42%, 47%, 50%, 74%, and 83% in particles ranging from 20nm to 200nm in sizecontributions in the 20, 50, 100, 150, and 200 nm size particles… respectively. ThereforeHence… ACl playsis…a significant role in increasingcritical factor to enhance…aerosol hygroscopicity, leading to the formation of trigger …og/haze formation …nder higher RH and colder atmospheric conditions as discussed in the previous section …

**Supprimé:** Similarly, …ADDIN CSL_CITATION { "citationItems" : [ { "id" : "ITEM-1", "itemData" : { "DOI" : "10.1038/s41561-020-00677-x", "ISSN" : "17520908", "abstract" : "Many cities in India experience severe deterioration of air quality in winter. Particulate matter is a key atmospheric pollutant that impacts millions of people. In particular, the high mass concentration of particulate matter reduces visibility, which has severely damaged the economy and endangered human lives. But the underlying chemical mechanisms and physical processes responsible for initiating haze and fog formation remain poorly understood. Here we present the measurement results of chemical composition of particulate matter in Delhi and Chennai. We find persistently high chloride in Delhi and episodically high chloride in Chennai. These measurements, combined with thermodynamic modelling, suggest that in the presence of excess ammonia in Delhi, high local emission of hydrochloric acid partitions into aerosol water. The highly water-absorbing and soluble chloride in the aqueous phase substantially enhances aerosol water uptake through co-condensation, which sustains particle growth, leading to haze and fog formation. We therefore suggest that the high local concentration of gas-phase hydrochloric acid, possibly …

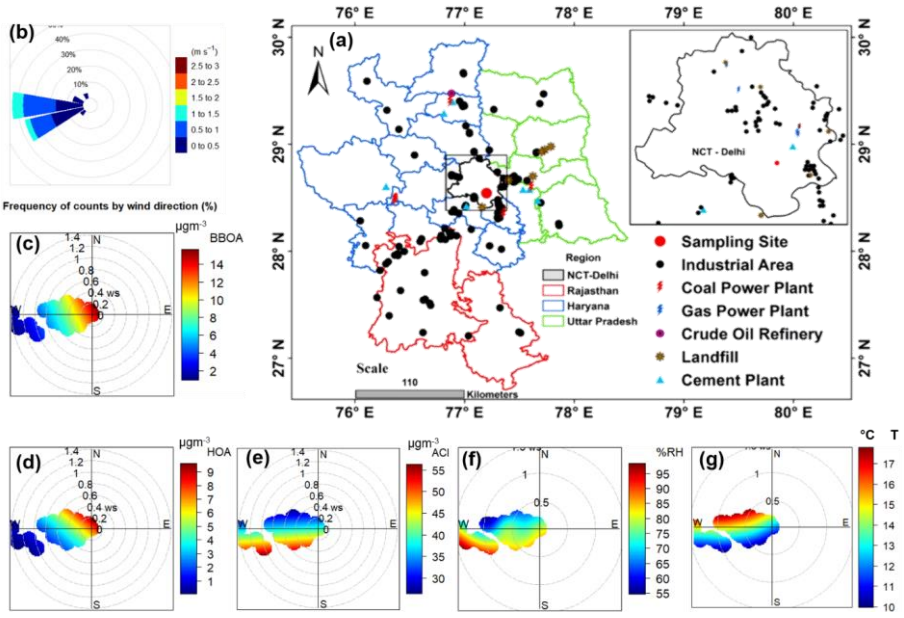


**Figure 7 Map of (a) Delhi showing various types of industries located in the region and nearby locations, (b) wind rose diagram and conditional bi-polar plots showing variation in mass concentration of (c) biomass burning OA (BBOA), (d) hydrocarbon like OA (HOA), (e) ammonium chloride (ACl), (f) % ambient relative humidity (RH), and (g) ambient temperature (T), with wind direction (WD) and wind speed (WS) during H-Cl events. A background map showing various industrial locations was adapted from Rai et al. (2020).**

### 3.2.4.2 High biomass burning (H-BB) Events

During the initial period of the field campaign (1-12 February), there were instances of high BB events. However, H-BB events were generally observed during the midnight (01:00 hours) to morning (08:00 hours) or evening (20:00 hours) to midnight (01:00 hours), and occasionally from evening (21:00 hours) to morning (11:00 hours). The surface wind circulations were predominantly from the W, W-WNW, and W-WSW directions (refer to Fig. S9b). The aerosol in this study was primarily sourced from local emissions. The aerosol constituents were mainly associated with slower wind circulations from landfill sites, industrial areas, and coal power plants, as shown in Fig. S9a. The PSCF analysis was justified by considering 48-hour air mass back trajectories, as shown in Fig. S10. The average GMD of the PNSD was nearly 87 nm. Additionally, the mean concentration of $SO_2$, NOx, and CO were at 4.7 ppb, 124.1 ppb, and 1.5 ppm, respectively. Therefore, it is possible that BBOA was contributed from the open local biomass burning activities at landfill sites or others sources. The H-BB event showed that

**Supprimé:** High BB events were noted d
**Supprimé:** of the field campaign
**Supprimé:** .
**Supprimé:** captured either
**Supprimé:** . Although, sometimes, it was continued
**Supprimé:** predominant
**Supprimé:** dominated by
**Supprimé:** ,
**Supprimé:** as
**Supprimé:** are
**Supprimé:** Further, it could justify t
**Supprimé:** potential source contribution function (
**Supprimé:** )
**Supprimé:** r
**Supprimé:** In a
**Supprimé:** concentrations
**Supprimé:** possibly
**Supprimé:** Organic aerosol in t

organic aerosol confined the largest fraction of BBOA, at 39%, followed by HOA at 28%. Fig. S9 (b, c, and d) clearly shows that BBOA and HOA have similar local source profiles but differ from the ACl source. Additionally, ACl was not found to have a strong association with ambient RH, but it was associated with emissions from a nearby coal power plant. However, the 48-hour air mass back trajectories indicate that the current city is also influenced by air masses from certain parts of Uttar Pradesh, Punjab, and Haryana. These states are potential hubs for crop residue burning, industrial activities and brick kilns, which contribute significantly to the presence of organic aerosols in $PM_1$, particularly during winter. The H-BB event captured a significant volume fraction, 71%, of OA in $PM_1$. BBOA contributed almost 39%, as shown in Fig. 9. A lower inorganic to OA ratio was a potential factor in decreasing the aerosol hygroscopicity during H-BB events. Additionally, the contribution of primary organic aerosol was enhanced during this event and, on average, increased to 67%. The hygroscopicity of the aerosol is inversely affected by organic aerosol loading. This observation was also reported by Mandariya et al. (2020) in Kanpur. The authors suggested that the hygroscopicity of the aerosol is adversely affected by primary biomass burning (BBOA) and hydrocarbon-like OA. BBOA was found to have a strong negative correlation with the hygroscopicity of 200 nm particles, supporting the conclusion. Apart from this, the Nucleation size particle (20 nm) exhibited a hygroscopicity parameter of 0.02 ± 0.02 with a mono mode GF-PDF with the unit mode (Fig. 8b) and consisted of 83.7 ± 18.6% nearly hydrophobic particles. Additionally, as the aerosol size increased, the hygroscopicity parameter ($\kappa_{H\text{-}TDMA\_90\%}$) significantly ($p<0.05$) increased due to the contribution of relatively secondary aerosol particles (GF>1.2) with increasing aerosol size. Approximately 54% of the accumulation size aerosol with a diameter of 100 nm is contributed by nearly hydrophobic particles (GF<1.2), while the remaining 46% is contributed by more hygroscopic particles (GF>1.2).

### 3.2.4.3 High-HOA (H-HOA) Events

H-HOA events were identified based on the considerable mass concentration and fraction of HOA in the organic aerosol. These periods were generally noted from 19:00 hr to 09:00 hr the following morning during February 22-23, February 26-27 February, March 4, and March 7-8, as indicated in Fig. 2. The average geometric mean diameter of the particle number size distribution was nearly 80 nm. Additionally, the mean concentrations of $SO_2$, NOx, and CO 4.3 ppb, 136.7 ppb, and 1.1 ppm, respectively. The potential impact of long-range transported aerosol was explored using PSCF. Air masses over Delhi, Haryana, and Uttar Pradesh were found to be potentially associated with hydrocarbon-like organic aerosols (Fig. S11). BBOA also followed a similar path as HOA. However, the potential area source of ACl was the nearby region of Delhi and Haryana. The loading of HOA was significantly ($p<0.05$) higher than in H-BB, H-Cl and Clean periods. However, emission sources were different

**Supprimé:** most considerable…argest fraction of BBOA, at 39%, of BBOA, …ollowed bying…HOA at,…28%. Figure… S9 (b, c, and d) clearly shows that BBOA and HOA have similar local source profiles but differ from the ACl source. AdditionallyMoreover… ACl was not found to have a stronggood…association with ambient RH, and …ut it was associated with emissions from a nearby coal power plant's emissions… However, the 48- …our air mass back indicated…that the current city was…s also influenced by air masses from certainsome…parts of Uttar Pradesh, Punjab, and Haryana. These states are the …otential hubs forof…crop residue burning, industrial activities and brick kilns,….which contribute significantly to the presence ofThese cities have a substantial fraction of…organic aerosolsOA …in $PM_1$ … particularlyand OA mainly affected by biomass activities…during winter. The H-BB event captured a significantconsiderable…volume fraction, 71%, of OA in $PM_1$ …and…BBOA contributed almost 39%, as shownillustrated…in the…Fig. 9. So,… lower inorganic to OA ratio was a potential factor in decreasing the aerosol hygroscopicity duringin…H-BB events. AdditionallyFurther… a primary organic aerosol …he contribution of primary organic aerosol was enhanced during this event and, on average, increasedraised…to 67%. The hygroscopicity of the aerosolOA loading…is inversely affecteds…by organic aerosol loadingthe aerosol's hygroscopicity… This observation was also reported by Mandariya et al. (2020) reported a similar observation …n Kanpur.,…and t…he authors suggested that the hygroscopicity of the aerosol is adversely affected bycontribution of…primary biomass burning (BBOA) and hydrocarbon-like OA adversely affects aerosol hygroscopicity… BBOA was found to have showed … stronggood…negative correlation with the hygroscopicity of 200 nm particles, supporting the following …onclusion. Apart from this, the Nucleation size particle (20 nm) exhibitedshowed…a hygroscopicity parameter of 0.02 ± 0.02 hygroscopicity parameter …ith a mono mode GF-PDF with the unit mode (Fig. 8b) and consisted offined…83.7 ± 18.6 … nearly hydrophobic particles. AdditionallyFurthermore… as the aerosol size increased, the hygroscopicity parameter ($\kappa_{H\text{-}TDMA\_90\%}$) enhanced …ignificantly ($p<0.05$) increased due toas…the contribution of relatively secondary aerosol particles (GF>1.2) increased …ith increasing aerosol size. Accumulation size aerosol, 100 nm contributed a…pproximately 54% of the accumulation size aerosol with a diameter of 100 nm is contributed by nearly hydrophobic particles (GF<1.2), while the remaining and …46% is contributed by more hygroscopic particles (GF>1.2) particl …

**Supprimé:** noted …enerally noted from19:00 hr to Morning 09:00 hr the following morning during February 22-23, and…February 26-27 February, and…arch 4, and March 7-8, March …s indicated in Fig. 2. The average geometric mean diameter of the particle number size distribution GMD of the PNSD …as nearly 80 nm. In a…ddtionally, the mean concentrations of $SO_2$, NOx, and CO concentrations were at 4.3 ppb, 136.7 ppb, and 1.1 ppm, respectively. The potential impact PSCF explore the probability of impacts …f long-range transported aerosol was explored using PSCF. Interestingly, it was observed that a…ir masses over Delhi, Haryana, and Uttar Pradesh were found to be potentially associated with hydrocarbon-like organic aerosolsOA…(Fig. S11). BBOA also followed a similar path as HOA. However, the potential area source of ACl was the nearby region of Delhi and Haryana. The loading of HOA loading …

during both H-HOA and H-BB periods. HOA may be a critical constituent in modulating aerosol hygroscopicity during these events, as it has been identified as a potential contributor to OA. HOA is typically considered hydrophobic (Duplissy et al., 2011), and therefore, its elevated contribution (41%) to OA could be responsible for the lower $\kappa$ observed during these events. The overall hygroscopicity of particles with sizes of 20, 50, 100, 150, and 200 nm was recorded as 0.01 ± 0.01, 0.06 ± 0.03, 0.11 ± 0.03, 0.14 ± 0.04, and 0.17 ± 0.05, respectively. The lower hygroscopicity of particles may be attributed to the predominant fractional contribution of primary aerosol particles (GF<1.2), as illustrated in Fig. 7(c). In general, OA constitutes the majority of the $PM_1$, with primary OA accounting for approximately 60% of the OA. However, the relative increase in the contribution of other more hygroscopic constituents, such as secondary organic aerosol (LO-OOA and MO-OOA), ACl, and AS, in the aerosol may help to balance the negative impact of high-HOA, which is limited by $\kappa$.

**3.2.4.5 Relatively Clean Period**

Clean events were recorded on February 24th, 25th, and March 5th–7th. The clean duration was from 9 PM to 11 AM. E and S-E winds dominated the relatively clean period, but pollution was associated with calm winds, as shown in Fig. S9. The average GMD of the PNSD was nearly 54 nm. Additionally, the mean concentrations of $SO_2$, NOx, and CO concentrations were at 4.2 ppb, 43.2 ppb, and 0.4 ppm, respectively. Similar sources were found for BBOA, HOA, and ACl, and they were all strongly associated with ambient relative humidity. The mean concentrations of organic aerosol, ACl, AN, and AS were 1.0 ± 6.4, 1.4 ± 1.1, 3.0 ± 1.5, and 4.4 ± 2.2 $\mu gm^{-3}$, respectively. These mass concentrations were significantly lower than in other specified periods. However, OA was still the dominant species, comprising 56% of the $PM_1$ volume, as shown in Fig. 9. Of all the factors contributing to OA, HOA was the dominant, accounting for 33%. However, secondary organic aerosol accounted for the majority of OA at 54.4%. Secondary OA is characterize by a relatively higher degree of oxidation, which positively affects OA hygroscopicity (Kim et al., 2017; Richard et al., 2011; Wu et al., 2013a). The mean hygroscopicity of particles with diameters of 20, 50, 100, 150, and 200 nm during the Clean period were observed to be 0.03 ± 0.02, 0.09 ± 0.04, 0.14 ± 0.06, 0.22 ± 0.09, and 0.27 ± 0.07, respectively. These values were significantly ($p<0.05$) different from each other. However, the hygroscopicity of the 200 nm accumulation particles was not significantly ($p>0.05$) higher than that of the 150 nm particles. The increase in hygroscopicity as particle size increases from 20 to 200 nm can also be attributed to the greater proportion of more hygroscopic particles (GF>1.2) compared to nearly hydrophobic or less hygroscopic particles (GF<1.2). The nucleation particles, with a size of 20 nm, were mostly composed of less hygroscopic particles (76.8 ± 21.7%). This indicates

**Supprimé:** As …OA may be a critical constituent in modulating aerosol hygroscopicity during these events, as it has been identified as awas the…potential contributor to OA., it is likely the critical constituent to modulate aerosol hygroscopicity in the region during these events.…HOA is typically mainly …onsidered hydrophobic (Duplissy et al., 2011),…and T…herefore, its elevated HOA …ontribution (41%) in…o OA could be responsible for the lower $\kappa$ observed duringin…these events. The overall hygroscopicity of particles with sizes of 20, 50, 100, 150, and 200 nm size particles …as recorded as 0.01 ± 0.01, 0.06 ± 0.03, 0.11 ± 0.03, 0.14 ± 0.04, and 0.17 ± 0.05, respectively. The lower hygroscopicity of particles may be attributed to the predominant fractional contribution of primary aerosol particles (GF<1.2), seems to be a reason for this lower hygroscopicity of particles, …s illustratedshown…in Ff…gure… 7(c). In generalOverall… OA predominantly constitutes the majority of fraction in …he $PM_1$, withand…primary OA accountingcontributed…for approximately 60% of thein…OA. However, the relative increasement…in the contribution of other more hygroscopic constituents, such as like…secondary organic aerosol (LO-OOA and MO-OOA), ACl, and ammonium sulfate (…S,)…in the aerosol may helppossible tried…to balance the negative impact of high-HOA, on ...

**Supprimé:** The …ebruary 24th …and…25th …of…February and Marchthe…5th,… 6th, and …th …of…The clean duration duration wasMarch were marked as…from 9 PM to 11 AM clean events… The night 21 hour to morning 11-hour duration was recorded as the clean duration. … and S-E windsThe relatively clean period was…predominantly dominated the relatively clean period, but by E, S-E winds; however,…pollution was associated with calm winds, as shownillustrated…in Fig. S9. The average GMD of the PNSD was nearly 54 nm. In a…ddtionally, the mean concentrations of $SO_2$, NOx, and CO concentrations were at 4.2 ppb, 43.2 ppb, and 0.4 ppm, respectively. Similar sources were found for All …BOA, HOA, and ACl, and they were all strongly associated were observed to be associated…with similar sources and found an excellent association with …mbient relative humidity. The mean concentrations of organic aerosol, ACl, AN, and AS wereas…observed at …1.0 ± 6.4, 1.4 ± 1.1, 3.0 ± 1.5, and 4.4 ± 2.2 $\mu gm^{-3}$, respectively. These mass concentrations were significantly lower than in other specified periods. However, OA was still the dominant species, comprisingwith…56% of by volume in …he $PM_1$,…volume, as shownindicated…in Fig. 9. OfAmong all the OA …actors contributing to OA, HOA was the pre…ominant, accounting forly dominated in OA with…33%.,…However,although…secondary organic aerosol accounted for the majority of OA atconfined the overall…54.4% of OA… Secondary OA is characterize by adefined with…relatively higher degree of oxidation, which oxidized OA, and the oxidation state of OA …ositively affectsimpacts…OA hygroscopicity (Kim et al., 2017; Richard et al., 2011; Wu et al., 2013a). The Clean period's mean hygroscopicity of particles with diameters of 20, 50, 100, 150, and 200 nm particles…uring the Clean period were observed to beat…0.03 ± 0.02, 0.09 ± 0.04, 0.14 ± 0.06, 0.22 ± 0.09, and 0.27 ± 0.07, respectively.,…These values were significantly ($p<0.05$) different fromto…each other. However, the hygroscopicity of the 200 nm accumulation particle'… (200 nm) hygroscopicity …as not significantly ($p>0.05$) higher than that of thee…150 nm particles. The increase in hygroscopicity as particle increment with …ize increases from 20 to 200 nm can also be attributed to ...

that there was an influence from fresh emission sources. On the other hand, Aitken (50 nm) and Accumulation (200 nm) size aerosols had a lower percentage of less hygroscopic particles, with 69.3 ± 14.7 and 25.4 ± 10.8, respectively. These results suggest that accumulation-size aerosols dominated secondary aerosols, which is also supported by their GF-PDF as shown in Fig. 8(a). Aerosol particles of nucleation size (20nm) exhibited a nearly mono-modal GF-PDF with a mode of unit growth factor. In contrast, as the aerosol size increased, the mode shifted towards the higher end and the GF-PDF shifted from unit to multi-mode.

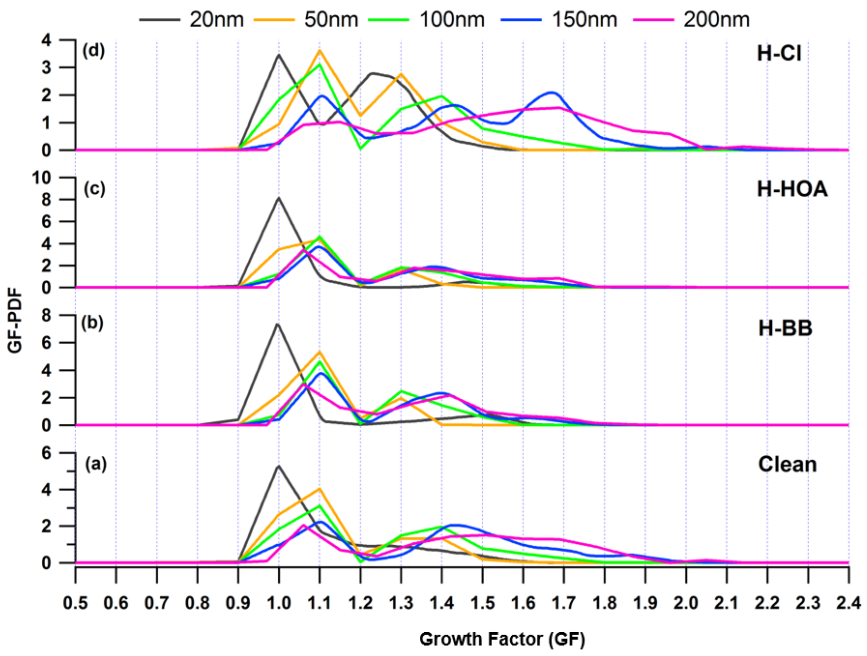


**Figure 8: Growth Factor Probability Density Function (GF-PDF) of 20, 50, 100, 150, and 200 nm aerosol particles for the (a) clean, (b) H-BB, (c) H-HOA, and H-Cl periods.**

### 3.2.4.6 Comparison of $\kappa$ for different events

We compared the hygroscopicity of aerosols during different periods using a 200 nm particle size that represents the bulk aerosol chemical composition. Additionally, in this study, the mode of the particle-volume size distribution ranged from 400 nm to 600 nm in dry mobility diameter. Therefore, 200 nm particles are the best choice for comparing hygroscopicity parameters among different periods, considering bulk aerosol composition. Additionally, a good Pearson's r value of 0.76 was found between $\kappa_{200nm\_90\%}$ and $\kappa_{chem\_90\%}$, which were derived



**Supprimé:** by…fresh emission sources.,…On the other hand, whereas, …itken (50 nm) and Accumulation (200 nm) size aerosols had a lower percentage of less hygroscopic particles,were confined…with 69.3 ± 14.7 and 25.4 ± 10.8 less hygroscopic particles… respectively. These results that point out that …ccumulation-size aerosols dominated secondary aerosols, which iscan…also supported by their GF-PDF as shown in Fig. 8(a). Aerosol particles of N…ucleation size aerosol particles …20nm) exhibitedshowed…a nearly mono- …odal GF-PDF with athe…mode of unit growth factor. In contrast, asthe…the aerosol size increased, the mode shifted towards the higher end as aerosol size increas ...

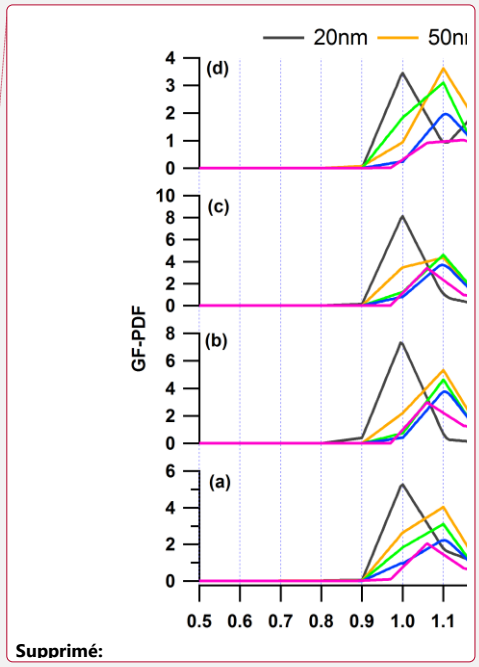


**Supprimé:**

**Supprimé:** onsidered…a 200 nm particle size that accumulation particle size particle …epresentsing…the bulk aerosol chemical composition. to compare the aerosol hygroscopicity among various periods.
in thise…present …tudy, the mode of the particle-volume size distribution ranged varied …rom 400 nm to 600 nm inparticle…dry mobility diameter. Therefore, 200 nm size accumulation …articles are the best choice forto…comparinge…hygroscopicity parameters among different periods, considering bulk aerosol composition. in various mentioned periods. In a…dditionally, a good Pearson's r value of,…0.76,…was found betweenamong ...

from the chemical composition of dry $PM_1$ particles measured by the ACSM using the ZSR mixing rule (Stokes and Robinson, 1966). This support our selection.

The event labeled H-Cl exhibited the highest value (0.36 ± 0.06) of $\kappa_{200nm\_90\%}$ compared to the events labeled H-BB (0.18 ± 0.04), H-HOA (0.17 ± 0.05), and Clean (0.27 ± 0.07), as shown in Fig. 9. Additionally, the average $\kappa_{200nm\_90\%}$ value for the H-Cl event was significantly ($p<0.05$) higher than that of the other events. A significant increase in Cl emissions in the Delhi region could lead to a substantial increase in the aerosol liquid water content. This increase in water content could result in higher aerosol hygroscopicity, which could further enhance cloud condensation nuclei formation. This, in turn, could potentially trigger haze/fog events in Delhi NCR (Gunthe et al., 2021). Controlling open trash/waste burning in the region could help minimize Cl emissions, which in turn could rduce the possibility of haze/fog formation during high atmospheric conditions. However, there was no significant difference ($p>0.05$) in $\kappa_{200nm\_90\%}$ values between H-BB and H-HOA events, possibly due to relative changes in primary, secondary OA, and inorganic species. In H-HOA events, the negative effect of a significantly higher fractional contribution of HOA to OA (41%) possibly balances with a positive impact of a 7% increase in secondary OA relative to H-BB. Several worldwide studies (Jimenez et al., 2009; Mandariya et al., 2019; Sun et al., 2013) have reported that secondary organic aerosol is associated with a higher O/C ratio. Additionally, several studies have found a positive correlation between the O/C ratio and $\kappa$ (Jimenez et al., 2009; Kim et al., 2020), as described earlier. Furthermore, a 5% decrease in ACl during H-HOA events may be offset by a 7% increase in AS fraction during H-BB events. Overall, the relative changes in aerosol constituents resulted in insignificant changes in $\kappa$ during H-BB and H-HOA periods. However, H-BB and H-HOA events showed significantly ($p<0.05$) lower hygroscopicity compared to a relatively cleaner atmosphere. The aerosol associated with relatively cleaner events had a higher inorganic-to-organic ratio. Additionally, during clean periods, the aerosol consisted of a significantly higher fraction of secondary organic aerosol. This could be the reason for the higher hygroscopicity associated with organic aerosol compared to other events. Studies worldwide (Aiken et al., 2008; Cerully et al., 2015b; Chakraborty et al., 2016b; Mandariya et al., 2019) have reported that organic aerosol loading has an inverse impact on the oxidation/aging process of OA. This results in higher hygroscopicity during relatively cleaner periods.

**Supprimé:** 's…chemical composition …easured by from the ACSM using based on…the ZSR mixing rule (Stokes and Robinson, 1966).,…This support which justifies …ur selectionchoice ...

**Supprimé:** H-Cl …vent labeled H-Cl exhibitednoted…the highest value (0.36 ± 0.06) of $\kappa_{200nm\_90\%}$ compared to the events labeledagainst…H-BB (0.18 ± 0.04), H-HOA (0.17 ± 0.05), and Clean (0.27 ± 0.07), events, …s shownillustrated…in Fig. 9. Additionally, T…he H-Cl event observed that the …verage $\kappa_{200nm\_90\%}$ value for the H-Cl event was significantly ($p<0.05$) higher than that of thethose observed in…other events. A significant increaseIt means that substantial increment…in Cl emissions in the Delhi region could lead to a substantial increase insignificantly enhance…the aerosol liquid water content. This increase in water content could result in leading to…higher aerosol hygroscopicity, which couldan…further enhancestrengthen…cloud condensation nuclei formation.,…This, in turn, could potentiallypossibly…triggering…haze/fog events in Delhi NCR (Gunthe et al., 2021). CThese results suggest that c…ntrolling the …pen trash/waste burning in the region help minimizecontrol…Cl emissions, which in turn could rduceleads to minimizing…the possibility of haze/fog formation possibility …uring high atmospheric conditions. However, there was no significantthe…difference ($p>0.05$) in $\kappa_{200nm\_90\%}$ values between H-BB and H-HOA events, was not observed significantly ($p>0.05$), …ossibly due to the changes in primary, secondary OA, and inorganic species. In the …-HOA events, the negative effect of a significantly higher fractional (41%) …ontribution of HOA to OA (41%) possibly balances with a positive impact of a 7% increasement…in secondary OA relative to H-BB. Several W…orldwide studies (Jimenez et al., 2009; Mandariya et al., 2019; Sun et al., 2013) have reported that secondary organic aerosol is associated with a higher O/C ratio.,…Additionallyand… several studies have found a positive correlation betweenreported that…the O/C ratio andpositively correlated to…$\kappa$ (Jimenez et al., 2009; Kim et 2020), as described in the …arlier text… Furthermore, aimpacts of…5% decreasement…in ACl during H-HOA may be offset by a 7% increase concerning H-BB event possibly managed by 7% increment …n AS fraction during H-BB events. Overall, these…relative changes in aerosol constituents resulted inworked to…insignificant changes in $\kappa$ during H-BB and H-HOA periods. HoweverNevertheless… H-BB and H-HOA events showed significantlywitnessed significant …($p<0.05$) lower hygroscopicity compared to a relatively cleaner atmosphere. The aerosol associated with relatively cleaner events hadwas with…a higher inorganic-to-organic ratio. In a…dditionally, the aerosol in…uring clean periods, the aerosol consistedmprised…of a significantly higher fraction of secondary organic aerosol.,…Thiswhich…could be the reason for the higher hygroscopicity associated with organic aerosol compared to other events. Studies W…orldwide (Aiken et al., 2008; Cerully et al., 2015b; Chakraborty et al., 2016b; Mandariya et al., 2019) studies …ave reported that organic aerosol loading has an inversely…impacts…on the oxidation/aging process of OA. This results inOverall, all these were responsible for…higher hygroscopicity duringin ...

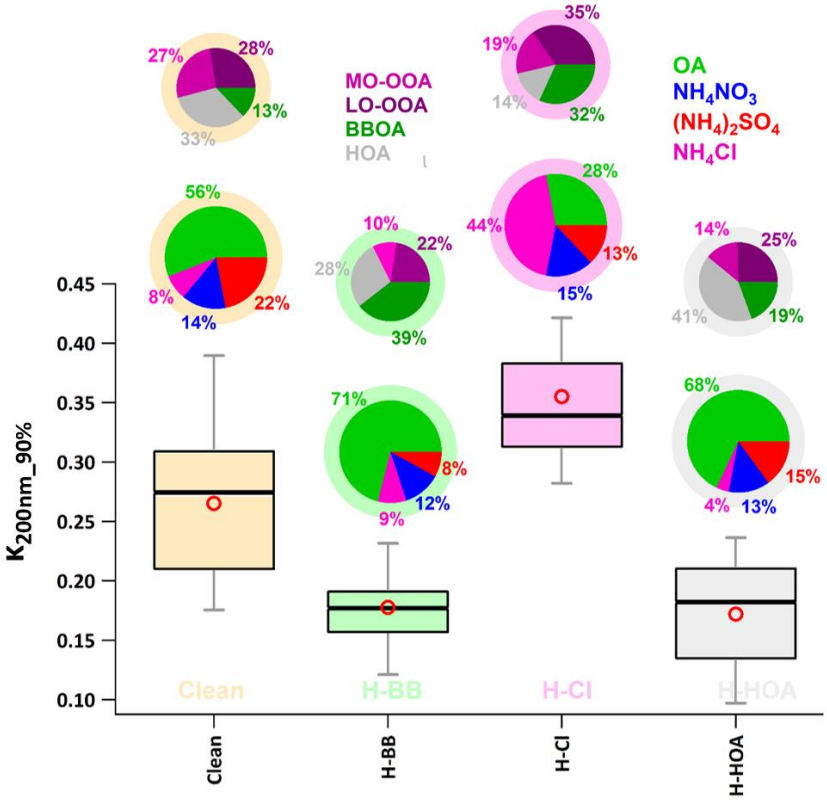


**Figure 9: Box plot showing variation in H-TDMA measured hygroscopic parameter of 200 nm size particles $\kappa_{H\text{-}TDMA}$ ($\kappa_{200nm\_90\%}$) in high biomass burning (H-BB), high-chloride (H-Cl), and high-hydrocarbon like organic aerosol (H-HOA) events. Different colors represent respective events in the plot. A bigger pie chart represents the overall average volume fractional contribution of various aerosol species indicated by color-coding. In addition, minor pie charts described the event average mass fractional contribution of different OA species in OA. Diffused ring color of the pie chart displays the respective event.**

## 4. Conclusions

The study examined the hygroscopicity of aerosol particles of various sizes (Nucleation - 20 nm, Aitken - 50 nm, and Accumulation - 150 and 200 nm) in Delhi during the winter months of February-March 2020. The research also identified differences in hygroscopicity, particularly in aerosols with higher levels of chloride, biomass burning, and hydrocarbon-like organic components. Delhi is known as one of the most polluted cities, particularly

**Supprimé:** present
**Supprimé:** investigated
**Supprimé:** temporal variation of
**Supprimé:** in
**Supprimé:** different
**Supprimé:** ,
**Supprimé:** namely Nucleation (20 nm), Aitken (50 nm), and Accumulation (150 and 200 nm) modes
**Supprimé:** period
**Supprimé:** is
**Supprimé:** highlighted variations
**Supprimé:** specifically
**Supprimé:** ,

during winter haze and fog events when it often experiences high levels of chloride pollution. This study reports on the temporal variations in size-specific hygroscopic parameters ($\kappa_{H\text{-}TDMA\_90\%}$) under sub-saturated conditions (90% RH) in Delhi for the first time. Additionally, it presents the hygroscopicity of nucleation and Aitken mode particles using HTDMA for the first time in India.

The $\kappa_{H\text{-}TDMA\_90\%}$ values observed for aerosol particles of 20 nm, 50 nm, 100 nm, 150 nm, and 200 nm ranged from 0.00 to 0.11 (with an average of 0.03 ± 0.02), 0.05 to 0.22 (0.11 ± 0.03), 0.05 to 0.30 (0.14 ± 0.04), 0.05 to 0.41 (0.18 ± 0.06), and 0.05 to 0.56 (0.22 ± 0.07), respectively. During the study period, it was observed that the average hygroscopicity parameter increased significantly with the size of the particles ($p<0.05$). The diurnal variations of $\kappa_{20nm\_90\%}$ and $\kappa_{50nm\_90\%}$ were dynamic, while larger accumulation mode particles showed a flatter diurnal pattern. This was due to the positive and negative effects of changes in the volume fraction of $NH_4Cl$ and organic aerosol in the aerosol with increasing particle size. The variation in $\kappa_{200nm\_90\%}$ was primarily associated with fluctuations in $NH_4Cl$ and OA, rather than $(NH_4)_2SO_4$. It is important to note that this evaluation is based on objective data and does not include any subjective evaluations

Pollution episodes were mainly linked to local biomass burning and industrial and waste-burning emissions in Delhi and nearby regions. The study primarily focused on the impacts of high biomass burning (H-BB), high hydrocarbon-like OA (H-HOA), and high chloride emissions (H-Cl) on aerosol hygroscopicity and compared them to cleaner periods. The period with H-Cl exhibited significantly higher hygroscopicity (0.35 ± 0.06) compared to the periods with H-BB (0.18 ± 0.04), H-HOA (0.17 ± 0.05), and the relatively cleaner period (0.27 ± 0.07). However, H-BB and H-HOA showed no significant difference in hygroscopicity but displayed lower hygroscopicity compared to the cleaner periods. This could be attributed to lower levels of organic aerosols and a higher ratio of inorganic-to-organic aerosol in the aerosol. The study found that an increase of 10% increase in chloride aerosol (ammonium chloride) significantly increased hygroscopicity, resulting in approximately 3 $\mu g\ m^{-3}$ higher aerosol liquid water content during high chloride events. This 10% increase in a high-volume fraction of ammonium chloride in aerosol significantly ($p<0.05$) enhanced aerosol hygroscopicity by 0.0041. The research indicates that chloride emissions are a significant concern in Delhi. These emissions enhance aerosol hygroscopicity, promote cloud formation during winter days, and contribute to fog and haze in the region. High levels of chloride in aerosols counteract the negative impact of high organic aerosol loading on cloud condensation nuclei activity. The study suggests that controlling open burning of waste materials could help reduce haze and fog events in Delhi during the winter months.

**Supprimé:** during winter haze and fog events. Consequently, t…his study reportsed…on the temporal variations in size-specific hygroscopic parameters ($\kappa_{H\text{-}TDMA\_90\%}$) under sub-saturated conditions (90% RH) in Delhi for the first time. AdditionallyFurthermore… it presentsed …

**Supprimé:** observed…$\kappa_{H\text{-}TDMA\_90\%}$ values observed for aerosol particles of 20 nm, 50 nm, 100 nm, 150 nm, and 200 nm ranged from 0.00 to 0.11 (with an average of 0.03 ± 0.02), for 20 nm aerosol particles, ….05 to 0.22 (0.11 ± 0.03) for 50 nm particles… 0.05 to 0.30 (0.14 ± 0.04) for 100 nm particles… 0.05 to 0.41 (0.18 ± 0.06) for 150 nm particles,… and 0.05 to 0.56 (0.22 ± 0.07) for 200 nm particles… respectively. During the study period, it was observed that the The …verage hygroscopicity parameter increased for the period …ignificantly increased …ith the size of the particles ($p<0.05$). The diurnal variations of …$_{20nm\_90\%}$ and $\kappa_{50nm\_90\%}$ weredisplayed…dynamic diurnal variations… while larger accumulation mode particles showedexhibited…a flatter diurnal pattern. This was due attributed …o the balancing positive and negative effects of changes in the volume fraction of $NH_4Cl$ and organic aerosol (OA) …n the aerosol with increasing particle size. Interestingly, t …

**Supprimé:** Furthermore, p…llution episodes were mainlypredominantly…linked to local biomass burning and industrial and waste-burning emissions in Delhi and nearby regions. The study primarily focused on highlighting …he impacts of high biomass burning (H-BB), high hydrocarbon-like OA (H-HOA), and high chloride emissions (H-Cl) on aerosol hygroscopicity and compared them to cleaner periods. The period with H-Cl period …xhibited significantly higher hygroscopicity (0.35 ± 0.06) compared to the periods with H-BB (0.18 ± 0.04), H-HOA (0.17 ± 0.05), and the relatively cleaner period (0.27 ± 0.07). However, H-BB and H-HOA showed no significant difference in hygroscopicity but displayed lower hygroscopicity compared to the cleaner periods. This could be attributed to lower levels of organic aerosols levels…and a higher ratio of inorganic-to-organic aerosol ratio …n the aerosol. The study found thatalso revealed that…an increase of 10% increase in chloride (ammonium chloride) in the aerosol …ignificantly increasedenhanced…hygroscopicity, resulting inleading to…approximately 3 $\mu g\ m^{-3}$ higher aerosol liquid water content during high chloride events. This 10% increase inenhancement of…a high-volume fraction of ammonium chloride in aerosol significantly ($p<0.05$) enhanced the aerosol hygroscopicity significantly ($p<0.05$) …y 0.0041. Furthermore, t…he research indicatessuggested…that emissions arewere…a significant concern in Delhi.,…These emissions enhanceenhancing …aerosol hygroscopicity, promoteing…cloud formation during winter days, and contributeing…to fog and haze in the region. High levels of chloride levels …n aerosols counteracted…the negative impact of high organic aerosolOA…loading on cloud condensation nuclei (CCN)…activity. The study suggestsConsequently,… the results indicated …

**Supporting Information**

Supplementary pieces of information are mentioned in the supplementary file.

**Data availability.** Data can be accessed at the following repository:

https://web.iitd.ac.in/~gazala/publications.html (Mandariya et al., 2023).

**Author contributions.** AKM: conceptualization, HTDMA data analysis, investigation, methodology, writing (original draft and review and editing). AA: operated aerosol instrumentation and collection of data on-board in Delhi, analysis of MPSS data, conceptualization, conceptualization, review and editing. MMVH: help in data collection. NAB: ACSM operation and data collection. KP: ACSM data analysis and PMF analysis. JSA: providing ACSM, review, and editing. LHR: ACSM, review, and editing. AW: experiment design, project administration, supervision, review, and editing. GH: operated aerosol instrumentation and collection of data on-board in Delhi, data analysis, methodology, funding acquisition, project administration, supervision, review and editing.

**Corresponding Author**

Gazala Habib (gazalahabib@civil.iitd.ac.in) and Alfred Wiedensohler (ali@tropos.de)

**Competing interests**

The authors declare that they have no conflict of interest.

**Acknowledgment**

The authors express their gratitude to Dr. Martin Gysel of the Aerosol Physics Group at the Paul Scherrer Institute in Switzerland for providing the TDMAinv toolkit for HTDMA data correction.

**REFERENCES**

Achtert, P., Birmili, W., Nowak, A., Wehner, B., Wiedensohler, A., Takegawa, N., Kondo, Y., Miyazaki, Y., Hu, M. and Zhu, T.: Hygroscopic growth of tropospheric particle number size distributions over the North China Plain, J. Geophys. Res., 114(8), D00G07, doi:10.1029/2008JD010921, 2009.

Aiken, A. C., Decarlo, P. F., Kroll, J. H., Worsnop, D. R., Huffman, J. A., Docherty, K. S., Ulbrich, I. M., Mohr, C., Kimmel, J. R., Sueper, D., Sun, Y., Zhang, Q., Trimborn, A., Northway, M., Ziemann, P. J., Canagaratna, M. R., Onasch, T. B., Alfarra, M. R., Prevot, A. S. H., Dommen, J., Duplissy, J., Metzger, A., Baltensperger, U. and Jimenez, J. L.: O/C and OM/OC ratios of primary, secondary, and ambient organic aerosols with high-resolution time-of-flight aerosol mass spectrometry, Environ. Sci. Technol., 42(12), 4478–4485, doi:10.1021/es703009q, 2008.



Supprimé: ¶

Mis en forme : Espace Avant : 12 pt, Après : 0 pt

Supprimé: H,

Supprimé: ,

Supprimé: ,

Supprimé: and

Supprimé: operated aerosol instrumentation and collection of data on-board in Delhi. KP analysed the ACSM data. AKM, AH, and GH conceptualized the structure of the manuscript. AKM analysed, evaluated H-TDMA data, and wrote the manuscript. AH analysed MPSS data. AKM, AH, KP, JSA, LHR, AW, and GH internally reviewed the manuscript and helped to write the manuscript.

Supprimé: thankful

Supprimé: ,

Supprimé: ,

Supprimé: ,

Supprimé: ,

3680 Albrecht, B. A.: Aerosols, Cloud Microphysics, and Fractional Cloudiness, Science (80-. )., 245(4923), 1227–
3681 1230, doi:10.1126/science.245.4923.1227, 1989.

3682 Arub, Z., Bhandari, S., Gani, S., Apte, J. S., Hildebrandt Ruiz, L. and Habib, G.: Air mass physiochemical
3683 characteristics over New Delhi: impacts on aerosol hygroscopicity and cloud condensation nuclei (CCN)
3684 formation, Atmos. Chem. Phys., 20(11), 6953–6971, doi:10.5194/acp-20-6953-2020, 2020.

3685 Bhandari, S., Gani, S., Patel, K., Wang, D. S., Soni, P., Arub, Z., Habib, G., Apte, J. S. and Hildebrandt Ruiz, L.:
3686 Sources and atmospheric dynamics of organic aerosol in New Delhi, India: insights from receptor modeling,
3687 Atmos. Chem. Phys., 20(2), 735–752, doi:10.5194/acp-20-735-2020, 2020.

3688 Bhattu, D. and Tripathi, S. N.: CCN closure study: Effects of aerosol chemical composition andmixing state, J.
3689 Geophys. Res., 120(2), 766–783, doi:10.1002/2014JD021978, 2015.

3690 Bhattu, D., Tripathi, S. N. and Chakraborty, A.: Deriving aerosol hygroscopic mixing state from size-resolved
3691 CCN activity and HR-ToF-AMS measurements, Atmos. Environ., 142, 57–70,
3692 doi:10.1016/j.atmosenv.2016.07.032, 2016.

3693 Cerully, K. M., Bougiatioti, A., Hite, J. R., Guo, H., Xu, L., Ng, N. L., Weber, R. and Nenes, A.: On the link
3694 between hygroscopicity, volatility, and oxidation state of ambient and water-soluble aerosols in the southeastern
3695 United States, Atmos. Chem. Phys., 15(15), 8679–8694, doi:10.5194/acp-15-8679-2015, 2015a.

3696 Cerully, K. M., Bougiatioti, A., Hite, J. R., Guo, H., Xu, L., Ng, N. L., Weber, R. and Nenes, A.: On the link
3697 between hygroscopicity, volatility, and oxidation state of ambient and water-soluble aerosols in the southeastern
3698 United States, Atmos. Chem. Phys., 15(15), 8679–8694, doi:10.5194/acp-15-8679-2015, 2015b.

3699 Chakraborty, A., Gupta, T. and Tripathi, S. N.: Combined effects of organic aerosol loading and fog processing
3700 on organic aerosols oxidation, composition, and evolution, Sci. Total Environ., 573, 690–698,
3701 doi:10.1016/j.scitotenv.2016.08.156, 2016a.

3702 Chakraborty, A., Gupta, T. and Tripathi, S. N.: Combined effects of organic aerosol loading and fog processing
3703 on organic aerosols oxidation, composition, and evolution, Sci. Total Environ., 573, 690–698,
3704 doi:10.1016/j.scitotenv.2016.08.156, 2016b.

3705 Chen, Y., Wang, Y., Nenes, A., Wild, O., Song, S., Hu, D., Liu, D., He, J., Hildebrandt Ruiz, L., Apte, J. S.,
3706 Gunthe, S. S. and Liu, P.: Ammonium Chloride Associated Aerosol Liquid Water Enhances Haze in Delhi, India,
3707 Environ. Sci. Technol., 56(11), 7163–7173, doi:10.1021/ACS.EST.2C00650, 2022.

3708 Draxler, Roland R., Hess, G. D.: Descrpition of the HYSPLIT_4 Modeling System, NOAA Techincal Memo.
3709 ERL ARL-224, (October 2004), 28 [online] Available from: http://arlsun.arlhq.noaa.gov/documents/reports/arl-
3710 224.pdf%5Cnhttp://www.ciecem.uhu.es/hysplitweb08/document/arl-224.pdf, 1997.

3711 Duplissy, J., De Carlo, P. F., Dommen, J., Alfarra, M. R., Metzger, A., Barmpadimos, I., Prevot, A. S. H.,
3712 Weingartner, E., Tritscher, T., Gysel, M., Aiken, A. C., Jimenez, J. L., Canagaratna, M. R., Worsnop, D. R.,
3713 Collins, D. R., Tomlinson, J. and Baltensperger, U.: Relating hygroscopicity and composition of organic aerosol
3714 particulate matter, Atmos. Chem. Phys., 11(3), 1155–1165, doi:10.5194/acp-11-1155-2011, 2011.

3715 Enroth, J., Mikkilä, J., Németh, Z., Kulmala, M. and Salma, I.: Wintertime hygroscopicity and volatility of
3716 ambient urban aerosol particles, Atmos. Chem. Phys., 18(7), 4533–4548, doi:10.5194/acp-18-4533-2018, 2018.

3717 Ervens, B., Turpin, B. J. and Weber, R. J.: Secondary organic aerosol formation in cloud droplets and aqueous
3718 particles (aqSOA): A review of laboratory, field and model studies, Atmos. Chem. Phys., 11(21), 11069–11102,
3719 doi:10.5194/acp-11-11069-2011, 2011.

3720 Fan, X., Liu, J., Zhang, F., Chen, L., Collins, D., Xu, W., Jin, X., Ren, J., Wang, Y., Wu, H., Li, S., Sun, Y. and
3721 Li, Z.: Contrasting size-resolved hygroscopicity of fine particles derived by HTDMA and HR-ToF-AMS
3722 measurements between summer and winter in Beijing: the impacts of aerosol aging and local emissions, Atmos.
3723 Chem. Phys., 20(2), 915–929, doi:10.5194/acp-20-915-2020, 2020.

3724 Fountoukis, C. and Nenes, A.: ISORROPIAII: A computationally efficient thermodynamic equilibrium model for

K+-Ca2+-Mg2+-NH4+-Na+-SO42--NO3--Cl--H2O aerosols, Atmos. Chem. Phys., 7(17), 4639–4659, doi:10.5194/acp-7-4639-2007, 2007.

Gani, S., Bhandari, S., Seraj, S., Wang, D. S., Patel, K., Soni, P., Arub, Z., Habib, G., Hildebrandt Ruiz, L. and Apte, J. S.: Submicron aerosol composition in the world's most polluted megacity: the Delhi Aerosol Supersite study, Atmos. Chem. Phys., 19(10), 6843–6859, doi:10.5194/acp-19-6843-2019, 2019.

Gunthe, S. S., Rose, D., Su, H., Garland, R. M., Achtert, P., Nowak, A., Wiedensohler, A., Kuwata, M., Takegawa, N., Kondo, Y., Hu, M., Shao, M., Zhu, T., Andreae, M. O. and Pöschl, U.: Cloud condensation nuclei (CCN) from fresh and aged air pollution in the megacity region of Beijing, Atmos. Chem. Phys., 11(21), 11023–11039, doi:10.5194/acp-11-11023-2011, 2011.

Gunthe, S. S., Liu, P., Panda, U., Raj, S. S., Sharma, A., Darbyshire, E., Reyes-Villegas, E., Allan, J., Chen, Y., Wang, X., Song, S., Pöhlker, M. L., Shi, L., Wang, Y., Kommula, S. M., Liu, T., Ravikrishna, R., McFiggans, G., Mickley, L. J., Martin, S. T., Pöschl, U., Andreae, M. O. and Coe, H.: Enhanced aerosol particle growth sustained by high continental chlorine emission in India, Nat. Geosci., 14(2), 77–84, doi:10.1038/s41561-020-00677-x, 2021.

Gupta, T. and Mandariya, A.: Sources of submicron aerosol during fog-dominated wintertime at Kanpur, Environ. Sci. Pollut. Res., 20(8), doi:10.1007/s11356-013-1580-6, 2013.

Gysel, M., Crosier, J., Topping, D. O., Whitehead, J. D., Bower, K. N., Cubison, M. J., Williams, P. I., Flynn, M. J., McFiggans, G. B. and Coe, H.: Closure study between chemical composition and hygroscopic growth of aerosol particles during TORCH2, Atmos. Chem. Phys., 7(24), 6131–6144, doi:10.5194/acp-7-6131-2007, 2007.

Gysel, M., McFiggans, G. B. and Coe, H.: Inversion of tandem differential mobility analyser (TDMA) measurements, J. Aerosol Sci., 40(2), 134–151, doi:10.1016/j.jaerosci.2008.07.013, 2009.

Hallquist, M., Wenger, J. C., Baltensperger, U., Rudich, Y., Simpson, D., Claeys, M., Dommen, J., Donahue, N. M., George, C., Goldstein, A. H., Hamilton, J. F., Herrmann, H., Hoffmann, T., Linuma, Y., Jang, M., Jenkin, M. E., Jimenez, J. L., Kiendler-Scharr, A., Maenhaut, W., McFiggans, G., Mentel, T. F., Monod, A., Pŕevôt, A. S. H., Seinfeld, J. H., Surratt, J. D., Szmigielski, R. and Wildt, J.: The formation, properties and impact of secondary organic aerosol: current and emerging issues, Atmos. Chem. Phys., 9(November 2008), 5155–5236, 2009.

Hong, J., Häkkinen, S. A. K., Paramonov, M., Äijälä, M., Hakala, J., Nieminen, T., Mikkilä, J., Prisle, N. L., Kulmala, M., Riipinen, I., Bilde, M., Kerminen, V. M. and Petäjä, T.: Hygroscopicity, CCN and volatility properties of submicron atmospheric aerosol in a boreal forest environment during the summer of 2010, Atmos. Chem. Phys., 14(9), 4733–4748, doi:10.5194/acp-14-4733-2014, 2014.

Hong, J., Kim, J., Nieminen, T., Duplissy, J., Ehn, M., Äijälä, M., Hao, L. Q., Nie, W., Sarnela, N., Prisle, N. L., Kulmala, M., Virtanen, A., Petäjä, T. and Kerminen, V. M.: Relating the hygroscopic properties of submicron aerosol to both gas- and particle-phase chemical composition in a boreal forest environment, Atmos. Chem. Phys., 15(20), 11999–12009, doi:10.5194/acp-15-11999-2015, 2015.

Hong, J., Xu, H., Tan, H., Yin, C., Hao, L., Li, F., Cai, M., Deng, X., Wang, N., Su, H., Cheng, Y., Wang, L., Petäjä, T. and Kerminen, V. M.: Mixing state and particle hygroscopicity of organic-dominated aerosols over the Pearl River Delta region in China, Atmos. Chem. Phys., 18(19), 14079–14094, doi:10.5194/acp-18-14079-2018, 2018.

Hu, D., Chen, J., Ye, X., Li, L. and Yang, X.: Hygroscopicity and evaporation of ammonium chloride and ammonium nitrate: Relative humidity and size effects on the growth factor, Atmos. Environ., 45(14), 2349–2355, doi:10.1016/j.atmosenv.2011.02.024, 2011.

Intergovernmental Panel on Climate Change: Climate Change 2021 – The Physical Science Basis, Cambridge University Press., 2023.

Jimenez, J. L., Canagaratna, M. R., Donahue, N. M., Prevot, A. S. H., Zhang, Q., Kroll, J. H., DeCarlo, P. F., Allan, J. D., Coe, H., Ng, N. L., Aiken, A. C., Docherty, K. S., Ulbrich, I. M., Grieshop, A. P., Robinson, A. L., Duplissy, J., Smith, J. D., Wilson, K. R., Lanz, V. A., Hueglin, C., Sun, Y. L., Tian, J., Laaksonen, A., Raatikainen,

Supprimé: ¶

T., Rautiainen, J., Vaattovaara, P., Ehn, M., Kulmala, M., Tomlinson, J. M., Collins, D. R., Cubison, M. J., Dunlea, E. J., Huffman, J. A., Onasch, T. B., Alfarra, M. R., Williams, P. I., Bower, K., Kondo, Y., Schneider, J., Drewnick, F., Borrmann, S., Weimer, S., Demerjian, K., Salcedo, D., Cottrell, L., Griffin, R., Takami, A., Miyoshi, T., Hatakeyama, S., Shimono, A., Sun, J. Y., Zhang, Y. M., Dzepina, K., Kimmel, J. R., Sueper, D., Jayne, J. T., Herndon, S. C., Trimborn, A. M., Williams, L. R., Wood, E. C., Middlebrook, A. M., Kolb, C. E., Baltensperger, U. and Worsnop, D. R.: Evolution of organic aerosols in the atmosphere, Science (80-. )., 326(5959), 1525–1529, doi:10.1126/science.1180353, 2009.

Kawana, K., Nakayama, T. and Mochida, M.: Hygroscopicity and CCN activity of atmospheric aerosol particles and their relation to organics: Characteristics of urban aerosols in Nagoya, Japan, J. Geophys. Res. Atmos., 121(8), 4100–4121, doi:10.1002/2015JD023213, 2016.

Kecorius, S., Vogl, T., Paasonen, P., Lampilahti, J., Rothenberg, D., Wex, H., Zeppenfeld, S., Van Pinxteren, M., Hartmann, M., Henning, S., Gong, X., Welti, A., Kulmala, M., Stratmann, F., Herrmann, H. and Wiedensohler, A.: New particle formation and its effect on cloud condensation nuclei abundance in the summer Arctic: a case study in the Fram Strait and Barents Sea, Atmos. Chem. Phys, 19, 14339–14364, doi:10.5194/acp-19-14339-2019, 2019.

Kim, N., Park, M., Yum, S. S., Park, J. S., Song, I. H., Shin, H. J., Ahn, J. Y., Kwak, K. H., Kim, H., Bae, G. N. and Lee, G.: Hygroscopic properties of urban aerosols and their cloud condensation nuclei activities measured in Seoul during the MAPS-Seoul campaign, Atmos. Environ., 153, 217–232, doi:10.1016/j.atmosenv.2017.01.034, 2017.

Kim, N., Yum, S. S., Park, M., Park, J. S., Shin, H. J. and Ahn, J. Y.: Hygroscopicity of urban aerosols and its link to size-resolved chemical composition during spring and summer in Seoul, Korea, Atmos. Chem. Phys., 20(19), 11245–11262, doi:10.5194/acp-20-11245-2020, 2020.

Kitamori, Y., Mochida, M. and Kawamura, K.: Assessment of the aerosol water content in urban atmospheric particles by the hygroscopic growth measurements in Sapporo, Japan, Atmos. Environ., 43(21), 3416–3423, doi:10.1016/j.atmosenv.2009.03.037, 2009.

Kroll, J. H., Donahue, N. M., Jimenez, J. L., Kessler, S. H., Canagaratna, M. R., Wilson, K. R., Altieri, K. E., Mazzoleni, L. R., Wozniak, A. S., Bluhm, H., Mysak, E. R., Smith, J. D., Kolb, C. E. and Worsnop, D. R.: Carbon oxidation state as a metric for describing the chemistry of atmospheric organic aerosol, Nat. Chem., 3(2), 133–139, doi:10.1038/nchem.948, 2011.

Li, H., Wang, Q., Shao, M., Wang, J., Wang, C., Sun, Y., Qian, X., Wu, H., Yang, M. and Li, F.: Fractionation of airborne particulate-bound elements in haze-fog episode and associated health risks in a megacity of southeast China, Environ. Pollut., 208, 655–662, doi:10.1016/j.envpol.2015.10.042, 2016.

Liu, J., Horowitz, L. W., Fan, S., Carlton, A. G. and Levy, H.: Global in-cloud production of secondary organic aerosols: Implementation of a detailed chemical mechanism in the GFDL atmospheric model AM3, J. Geophys. Res. Atmos., 117(D15), n/a-n/a, doi:10.1029/2012JD017838, 2012.

Lohmann, U. and Feichter, J.: Global indirect aerosol effects: a review, Atmos. Chem. Phys., 5(3), 715–737, doi:10.5194/acp-5-715-2005, 2005.

Mandariya, A. K., Gupta, T. and Tripathi, S. N.: Effect of aqueous-phase processing on the formation and evolution of organic aerosol (OA) under different stages of fog life cycles, Atmos. Environ., 206(November 2018), 60–71, doi:10.1016/j.atmosenv.2019.02.047, 2019.

Mandariya, A. K., Tripathi, S. N., Gupta, T. and Mishra, G.: Wintertime hygroscopic growth factors (HGFs) of accumulation mode particles and their linkage to chemical composition in a heavily polluted urban atmosphere of Kanpur at the Centre of IGP, India: Impact of ambient relative humidity, Sci. Total Environ., 704, 135363, doi:10.1016/j.scitotenv.2019.135363, 2020a.

Mandariya, A. K., Tripathi, S. N., Gupta, T. and Mishra, G.: Wintertime hygroscopic growth factors (HGFs) of accumulation mode particles and their linkage to chemical composition in a heavily polluted urban atmosphere of Kanpur at the Centre of IGP, India: Impact of ambient relative humidity, Sci. Total Environ., 704, doi:10.1016/j.scitotenv.2019.135363, 2020b.

Massling, A., Leinert, S., Wiedensohler, A. and Covert, D.: Hygroscopic growth of sub-micrometer and one-micrometer aerosol particles measured during ACE-Asia, Atmos. Chem. Phys, 7, 3249–3259 [online] Available from: www.atmos-chem-phys.net/7/3249/2007/ (Accessed 30 October 2022), 2007.

Maßling, A., Wiedensohler, A., Busch, B., Neusüß, C., Neusüß, N., Quinn, P., Bates, T. and Covert, D.: Atmospheric Chemistry and Physics Hygroscopic properties of different aerosol types over the Atlantic and Indian Oceans, Atmos. Chem. Phys, 3, 1377–1397 [online] Available from: www.atmos-chem-phys.org/acp/3/1377/ (Accessed 30 October 2022), 2003.

Massoli, P., Lambe, A. T., Ahern, A. T., Williams, L. R., Ehn, M., Mikkilä, J., Canagaratna, M. R., Brune, W. H., Onasch, T. B., Jayne, J. T., Petäjä, T., Kulmala, M., Laaksonen, A., Kolb, C. E., Davidovits, P. and Worsnop, D. R.: Relationship between aerosol oxidation level and hygroscopic properties of laboratory generated secondary organic aerosol (SOA) particles, Geophys. Res. Lett., 37(24), 1–5, doi:10.1029/2010GL045258, 2010.

McFiggans, G., Artaxo, P., Baltensperger, U., Coe, H., Facchini, M. C., Feingold, G., Fuzzi, S., Gysel, M., Laaksonen, A., Lohmann, U., Mentel, T. F., Murphy, D. M., O'Dowd, C. D., Snider, J. R. and Weingartner, E.: The effect of physical and chemical aerosol properties on warm cloud droplet activation, Atmos. Chem. Phys., 6(9), 2593–2649, doi:10.5194/acp-6-2593-2006, 2006.

McNeill, V. F.: Aqueous organic chemistry in the atmosphere: Sources and chemical processing of organic aerosols, Environ. Sci. Technol., 49(3), 1237–1244, doi:10.1021/es5043707, 2015.

Mei, F., Setyan, A., Zhang, Q. and Wang, J.: CCN activity of organic aerosols observed downwind of urban emissions during CARES, Atmos. Chem. Phys., 13(24), 12155–12169, doi:10.5194/acp-13-12155-2013, 2013.

Ng, N. L., Herndon, S. C., Trimborn, A., Canagaratna, M. R., Croteau, P. L., Onasch, T. B., Sueper, D., Worsnop, D. R., Zhang, Q., Sun, Y. L. and Jayne, J. T.: An Aerosol Chemical Speciation Monitor (ACSM) for routine monitoring of the composition and mass concentrations of ambient aerosol, Aerosol Sci. Technol., 45(7), 780–794, doi:10.1080/02786826.2011.560211, 2011.

Ogawa, S., Setoguchi, Y., Kawana, K., Nakayama, T., Ikeda, Y., Sawada, Y., Matsumi, Y. and Mochida, M.: Hygroscopicity of aerosol particles and CCN activity of nearly hydrophobic particles in the urban atmosphere over Japan during summer, J. Geophys. Res., 121(12), 7215–7234, doi:10.1002/2015JD024636, 2016.

Petit, J. E., Favez, O., Albinet, A. and Canonaco, F.: A user-friendly tool for comprehensive evaluation of the geographical origins of atmospheric pollution: Wind and trajectory analyses, Environ. Model. Softw., 88, 183–187, doi:10.1016/j.envsoft.2016.11.022, 2017.

Petters, M. D. and Kreidenweis, S. M.: A single parameter representation of hygroscopic growth and cloud condensation nucleus activity, Atmos. Chem. Phys. Atmos. Chem. Phys., 7, 1961–1971, doi:10.5194/acp-7-1961-2007, 2007.

Prakash, J., Lohia, T., Mandariya, A. K., Habib, G., Gupta, T. and Gupta, S. K.: Chemical characterization and quantitativ e assessment of source-specific health risk of trace metals in PM1.0 at a road site of Delhi, India, Environ. Sci. Pollut. Res., 25(9), 8747–8764, doi:10.1007/s11356-017-1174-9, 2018.

Pringle, K. J., Tost, H., Pozzer, A., Pöschl, U. and Lelieveld, J.: Global distribution of the effective aerosol hygroscopicity parameter for CCN activation, Atmos. Chem. Phys., 10(12), 5241–5255, doi:10.5194/acp-10-5241-2010, 2010.

Rai, P., Furger, M., El Haddad, I., Kumar, V., Wang, L., Singh, A., Dixit, K., Bhattu, D., Petit, J.-E., Ganguly, D., Rastogi, N., Baltensperger, U., Tripathi, S. N., Slowik, J. G. and Prévôt, A. S. H.: Real-time measurement and source apportionment of elements in Delhi's atmosphere, Sci. Total Environ., 742, 140332, doi:10.1016/j.scitotenv.2020.140332, 2020.

Randall, D A; Wood, R A; Bony, S; Colman, R; Fichefet, T; Fyfe, J; Kattsov, V; Pitman, A; Shukla, J; Srinivasan, J; Stouffer, R J; Sumi, A; Taylor, K. E.: Climate Models and Their Application, Clim. Chang. 2007 Phys. Sci. Basis. Contrib. Work. Gr. I to Fourth Assess. Rep. Intergov. Panel Clim. Chang. Ed. by S. Solomon al., Cambridge Univ. Press. Cambridge, U. K., New York., Chapter 8(United Kingdom: N. p., p.2007. Web.), 590–662, doi:http://www.ipcc.ch/pdf/assessment-report/ar4/wg1/ar4-wg1-chapter8.pdf, 2007.

Richard, A., Gianini, M. F. D., Mohr, C., Furger, M., Bukowiecki, N. and Minguill, M. C.: and Physics Source apportionment of size and time resolved trace elements and organic aerosols from an urban courtyard site in Switzerland, , 8945–8963, doi:10.5194/acp-11-8945-2011, 2011.

Seinfeld, J. H. and Pandis, S. N.: Atmospheric cemistry and physics: From air pollution to climate change, Second edi., John Wiley & Sons, Inc., 2006.

Shukla, A. K., Lalchandani, V., Bhattu, D., Dave, J. S., Rai, P., Thamban, N. M., Mishra, S., Gaddamidi, S., Tripathi, N., Vats, P., Rastogi, N., Sahu, L., Ganguly, D., Kumar, M., Singh, V., Gargava, P. and Tripathi, S. N.: Real-time quantification and source apportionment of fine particulate matter including organics and elements in Delhi during summertime, Atmos. Environ., 261, 118598, doi:10.1016/J.ATMOSENV.2021.118598, 2021.

Sjogren, S., Gysel, M., Weingartner, E., Baltensperger, U., Cubison, M. J. and Coe, H.: Hygroscopic growth and water uptake kinetics of two-phase aerosol particles consisting of ammonium sulfate , adipic and humic acid mixtures, , 38, 157–171, doi:10.1016/j.jaerosci.2006.11.005, 2007.

Sjogren, S., Gysel, M., Weingartner, E., Alfarra, M. R., Duplissy, J., Cozic, J., Crosier, J. and Coe, and U. B.: Hygroscopicity of the submicrometer aerosol at the high-alpine site Jungfraujoch, 3580m a.s.l., Switzerland, , 7231–7249, doi:10.5194/acp-12-7231-2012, 2012.

Stokes, R. H. and Robinson, R. A.: Interactions in Aqueous Nonelectrolyte Solutions. I. Solute-Solvent Equilibria, J. Phys. Chem., 70(7), 2126–2131, doi:10.1021/j100879a010, 1966.

Su, H., Rose, D., Cheng, Y. F., Gunthe, S. S., Massling, A., Stock, M., Wiedensohler, A., Andreae, M. O. and Pöschl, U.: Hygroscopicity distribution concept for measurement data analysis and modeling of aerosol particle mixing state with regard to hygroscopic growth and CCN activation, Atmos. Chem. Phys, 10, 7489–7503, doi:10.5194/acp-10-7489-2010, 2010.

Sun, Y., Wang, Z., Fu, P., Jiang, Q., Yang, T., Li, J. and Ge, X.: The impact of relative humidity on aerosol composition and evolution processes during wintertime in Beijing , China, Atmos. Environ., 77, 927–934, doi:10.1016/j.atmosenv.2013.06.019, 2013.

Sun, Y., Du, W., Fu, P., Wang, Q., Li, J., Ge, X., Zhang, Q., Zhu, C., Ren, L., Xu, W., Zhao, J., Han, T., Worsnop, D. R. and Wang, Z.: Primary and secondary aerosols in Beijing in winter: Sources, variations and processes, Atmos. Chem. Phys., 16(13), 8309–8329, doi:10.5194/acp-16-8309-2016, 2016.

Swietlicki, E., Hansson, H. C., Hämeri, K., Svenningsson, B., Massling, A., Mcfiggans, G., Mcmurry, P. H., Petäjä, T., Tunved, P., Gysel, M., Topping, D., Weingartner, E., Baltensperger, U., Rissler, J., Wiedensohler, A. and Kulmala, M.: Hygroscopic properties of submicrometer atmospheric aerosol particles measured with H-TDMA instruments in various environments—a review, Tellus B Chem. Phys. Meteorol., 60(3), 432–469, doi:10.1111/j.1600-0889.2008.00350.x, 2008.

Tang, I. N. and Munkelwitz, H. R.: Water activities, densities, and refractive indices of aqueous sulfates and sodium nitrate droplets of atmospheric importance, J. Geophys. Res., 99(D9), 18801, doi:10.1029/94JD01345, 1994.

Tobler, A., Bhattu, D., Canonaco, F., Lalchandani, V., Shukla, A., Thamban, N. M., Mishra, S., Srivastava, A. K., Bisht, D. S., Tiwari, S., Singh, S., Močnik, G., Baltensperger, U., Tripathi, S. N., Slowik, J. G. and Prévôt, A. S. H.: Chemical characterization of PM2.5 and source apportionment of organic aerosol in New Delhi, India, Sci. Total Environ., 745, 140924, doi:10.1016/J.SCITOTENV.2020.140924, 2020.

Topping, D. O. and McFiggans, G.: Tight coupling of particle size, number and composition in atmospheric cloud droplet activation, Atmos. Chem. Phys., 12(7), 3253–3260, doi:10.5194/acp-12-3253-2012, 2012.

Tritscher, T., Jurnyi, Z., Martin, M., Chirico, R., Gysel, M., Heringa, M. F., Decarlo, P. F., Sierau, B., Prévt, A. S. H., Weingartner, E. and Baltensperger, U.: Changes of hygroscopicity and morphology during ageing of diesel soot, Environ. Res. Lett., 6(3), doi:10.1088/1748-9326/6/3/034026, 2011.

Wang, X., Shen, X. J., Sun, J. Y., Zhang, X. Y., Wang, Y. Q., Zhang, Y. M., Wang, P., Xia, C., Qi, X. F. and Zhong, J. T.: Size-resolved hygroscopic behavior of atmospheric aerosols during heavy aerosol pollution episodes

in Beijing in December 2016, , 194(September), 188–197, doi:10.1016/j.atmosenv.2018.09.041, 2018a.

Wang, Y., Wu, Z., Ma, N., Wu, Y., Zeng, L., Zhao, C. and Wiedensohler, A.: Statistical analysis and parameterization of the hygroscopic growth of the sub-micrometer urban background aerosol in Beijing, Atmos. Environ., 175(December 2017), 184–191, doi:10.1016/j.atmosenv.2017.12.003, 2018b.

Wester, P., Mishra, A., Mukherji, A., Shrestha, A. B. and Change, C.: The Hindu Kush Himalaya Assessment, edited by P. Wester, A. Mishra, A. Mukherji, and A. B. Shrestha, Springer International Publishing, Cham., 2019.

Wu, Z. J., Poulain, L., Henning, S., Dieckmann, K., Birmili, W., Merkel, M., van Pinxteren, D., Spindler, G., Müller, K., Stratmann, F., Herrmann, H. and Wiedensohler, A.: Relating particle hygroscopicity and CCN activity to chemical composition during the HCCT-2010 field campaign, Atmos. Chem. Phys., 13(16), 7983–7996, doi:10.5194/acp-13-7983-2013, 2013a.

Wu, Z. J., Poulain, L., Henning, S., Dieckmann, K., Birmili, W., Merkel, M., Van Pinxteren, D., Spindler, G., Stratmann, F., Herrmann, H. and Wiedensohler, A.: Sciences ess Atmospheric Chemistry and Physics Climate of the Past Geoscientific Instrumentation Methods and Data Systems Relating particle hygroscopicity and CCN activity to chemical composition during the HCCT-2010 field campaign, Atmos. Chem. Phys, 13, 7983–7996, doi:10.5194/acp-13-7983-2013, 2013b.

Wu, Z. J., Zheng, J., Shang, D. J., Du, Z. F., Wu, Y. S., Zeng, L. M., Wiedensohler, A. and Hu, M.: Particle hygroscopicity and its link to chemical composition in the urban atmosphere of Beijing , China , during summertime, , 1123–1138, doi:10.5194/acp-16-1123-2016, 2016.

Yeung, M. C., Lee, B. P., Li, Y. J. and Chan, C. K.: Simultaneous HTDMA and HR-ToF-AMS measurements at the HKUST supersite in Hong Kong in 2011, J. Geophys. Res., 119(16), 9864–9883, doi:10.1002/2013JD021146, 2014.

Zhang, Q., Jimenez, J. L., Worsnop, D. R. and Canagaratna, M.: A Case Study of Urban Particle Acidity and Its Influence on Secondary Organic Aerosol, Environ. Sci. Technol., 41(9), 3213–3219, doi:10.1021/es061812j, 2007.

Zhang, S. L., Ma, N., Kecorius, S., Wang, P. C., Hu, M., Wang, Z. B., Größ, J., Wu, Z. J. and Wiedensohler, A.: Mixing state of atmospheric particles over the North China Plain, Atmos. Environ., 125, 152–164, doi:10.1016/J.ATMOSENV.2015.10.053, 2016.

Zhang, Y., Tang, L., Yu, H., Wang, Z., Sun, Y., Qin, W., Chen, W., Chen, C., Ding, A., Wu, J., Ge, S. and Chen, C.: Chemical composition , sources and evolution processes of aerosol at an urban site in Yangtze River Delta , China during wintertime, Atmos. Environ., 123, 339–349, doi:10.1016/j.atmosenv.2015.08.017, 2015.

Zhao, P., Du, X., Su, J., Ding, J. and Dong, Q.: Aerosol hygroscopicity based on size-resolved chemical compositions in Beijing, Sci. Total Environ., 716, 137074, doi:10.1016/J.SCITOTENV.2020.137074, 2020.